

## Amphiphilic Poly(esteracetal)s as Dual pH- and Enzyme Responsive Micellar Immunodrug Delivery Systems

– Supplementary Information –

Leon Bixenmann,<sup>a</sup> Judith Stickdorn<sup>a</sup> and Lutz Nuhn<sup>a,\*</sup>

<sup>a</sup> *Max Planck Institute for Polymer Research, Ackermannweg 10, 55128 Mainz, Germany.*

\* *E-mail: lutz.nuhn@mpip-mainz.mpg.de. Tel: +49 6131-379-311.*

### Content

Analytical data of 2-methyl-1,3-dioxan-4-one (MDO) .....	2
Analytical data of Poly(pyrene butanol-MDO):.....	4
Analytical data of mPEG <sub>48</sub> - <i>b</i> -poly(MDO) block copolymers:.....	11
Block copolymer self-assembly:.....	24
Dual pH-responsive degradation .....	28
Enzymatic degradation studies .....	32
Loading and release studies.....	35
Application as immune drug delivery system .....	41

## Analytical data of 2-methyl-1,3-dioxan-4-one (MDO)

### <sup>1</sup>H-NMR of MDO

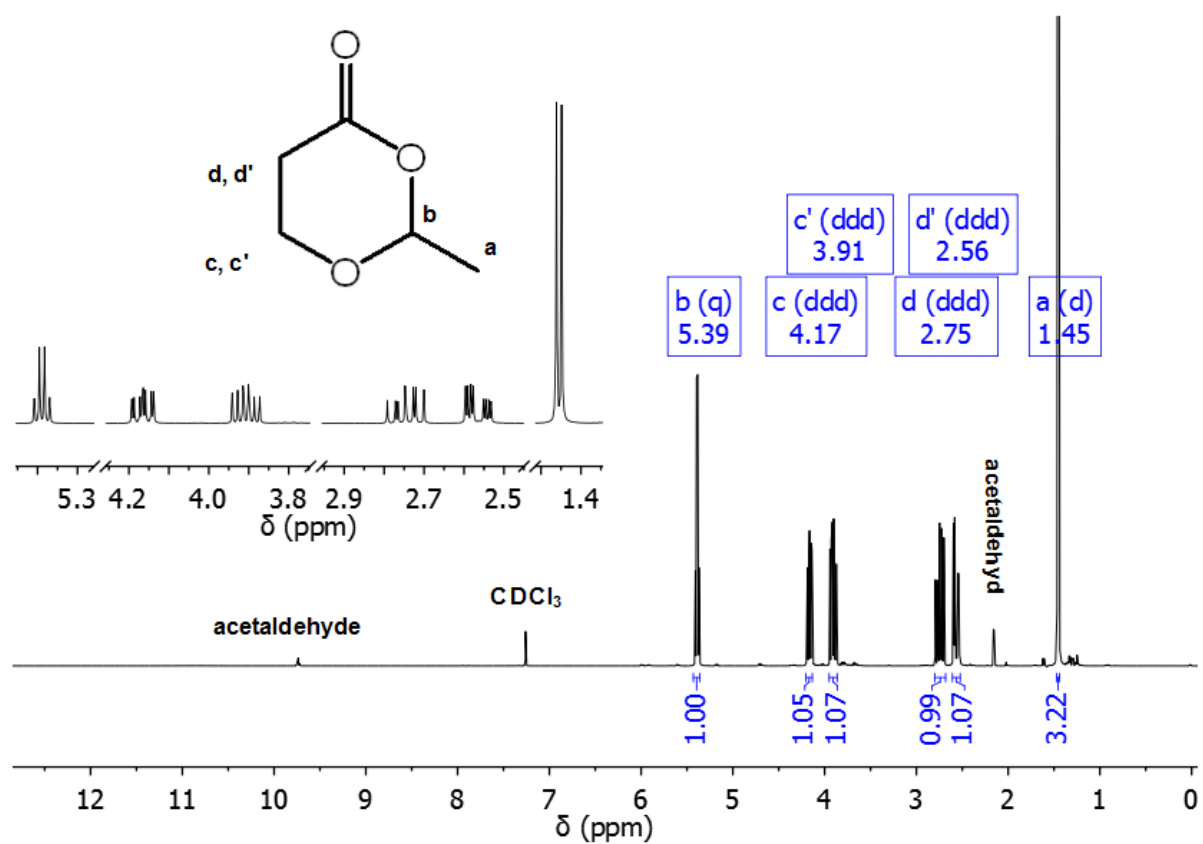


Figure S 1: <sup>1</sup>H-NMR (400 MHz) of 2-methyl-1,3-dioxan-4-one in CDCl<sub>3</sub>.

### <sup>13</sup>C-NMR of MDO

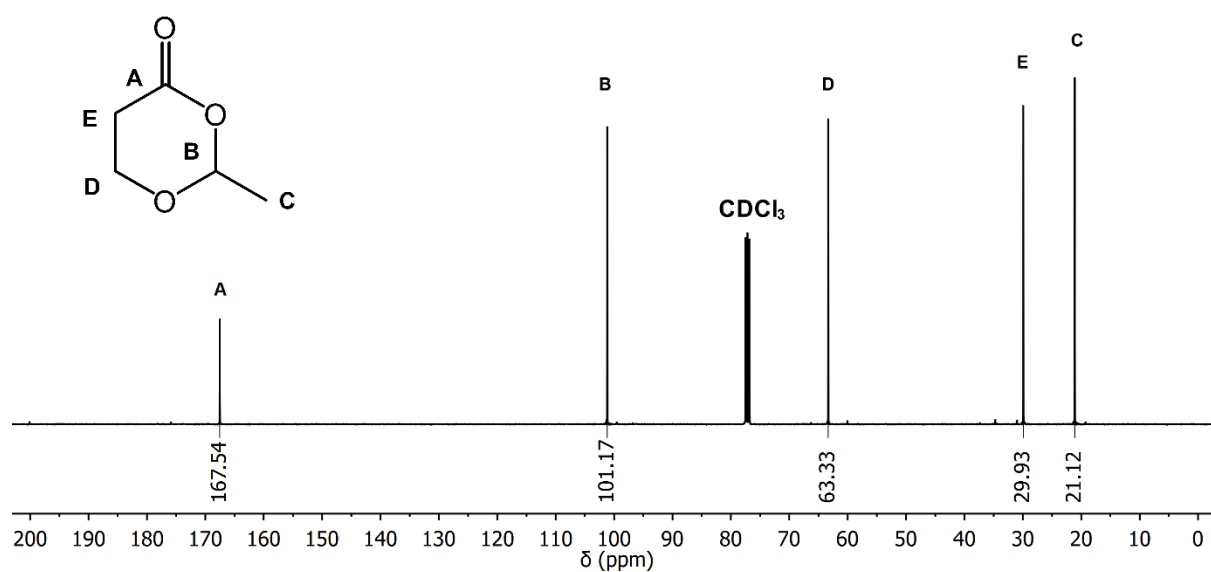


Figure S 2: <sup>13</sup>C-NMR (100 MHz) of 2-methyl-1,3-dioxan-4-one in CDCl<sub>3</sub>.

### $^1\text{H}$ , $^1\text{H}$ -COSY NMR of MDO

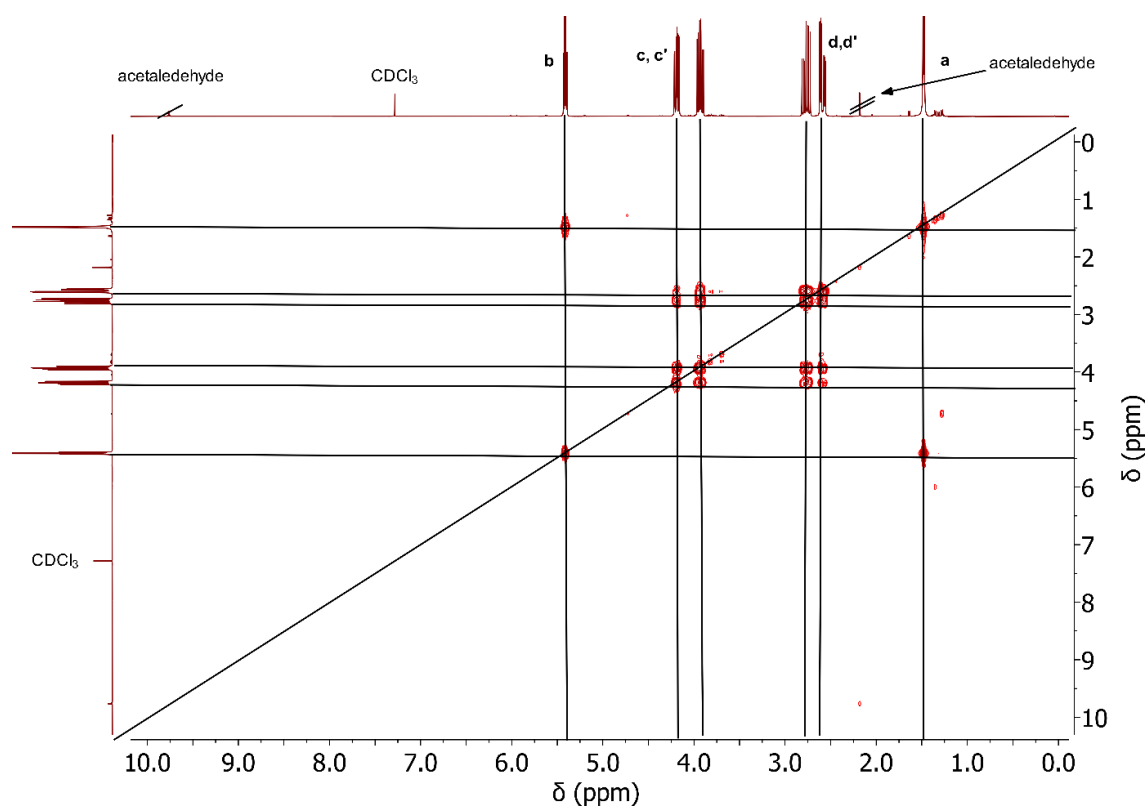


Figure S 3:  $^1\text{H}$ -NMR derived COSY NMR analysis of 2-methyl-1,3-dioxan-4-one in  $\text{CDCl}_3$ .

### $^1\text{H}$ , $^{13}\text{C}$ -HSQC NMR of MDO

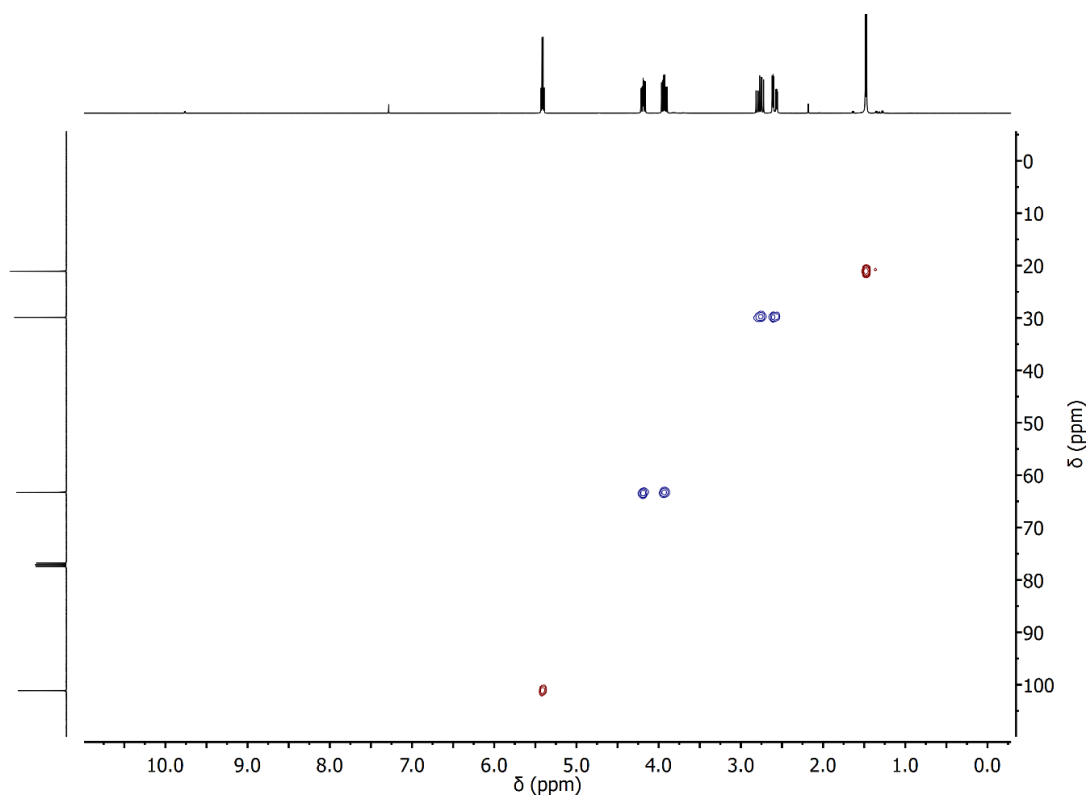
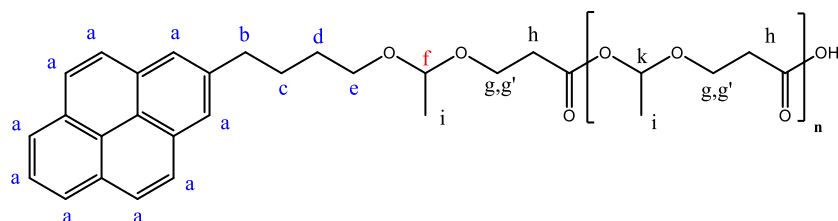


Figure S 4: HSQC NMR analysis of 2-methyl-1,3-dioxan-4-one in  $\text{CDCl}_3$ .

Analytical data of Poly(pyrene butanol-MDO):

**<sup>1</sup>H-NMR of poly(pyrene butanol-MDO) synthesized at room temperature**

Molecular structure of P(MDO):



Molecular structure of P(MDO) with incorporation of polyester units:

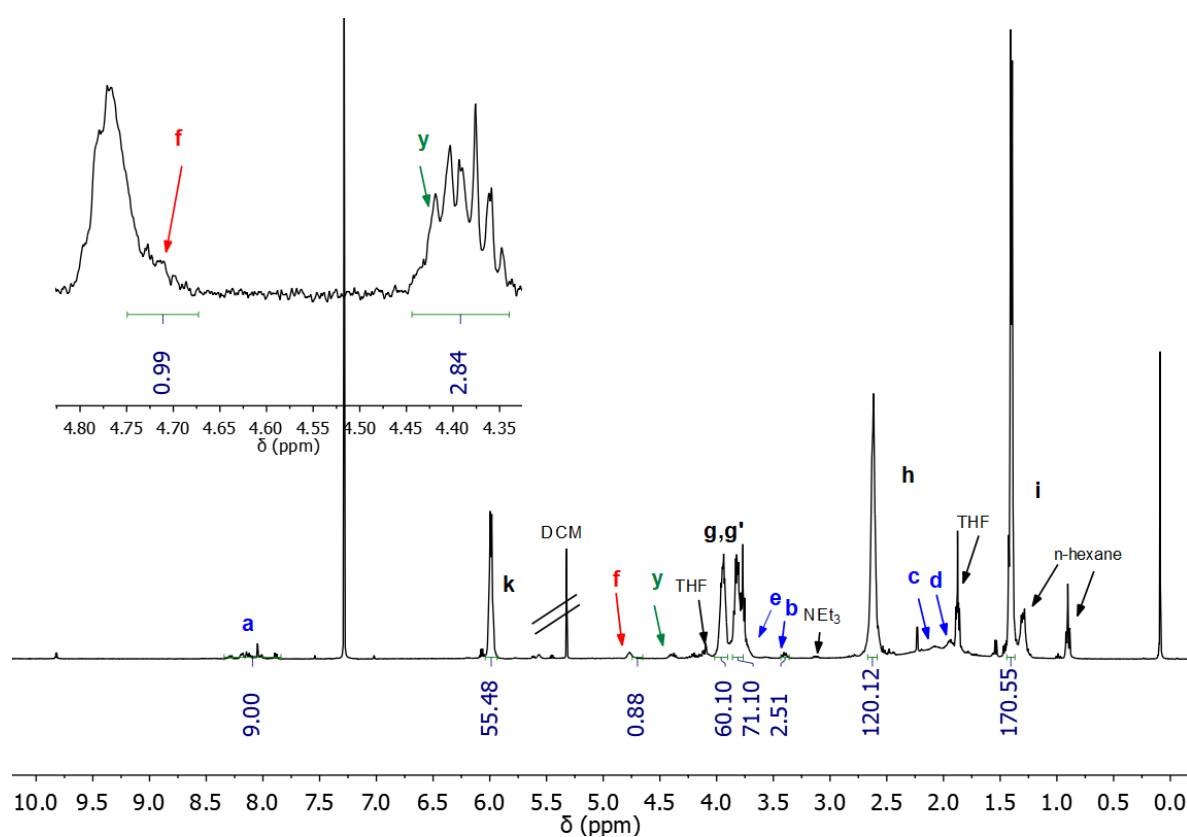
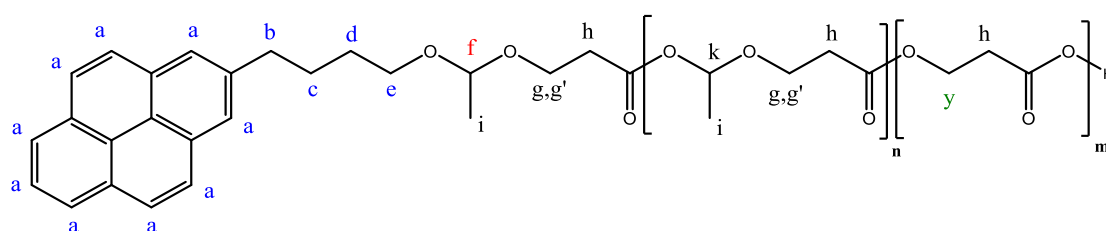
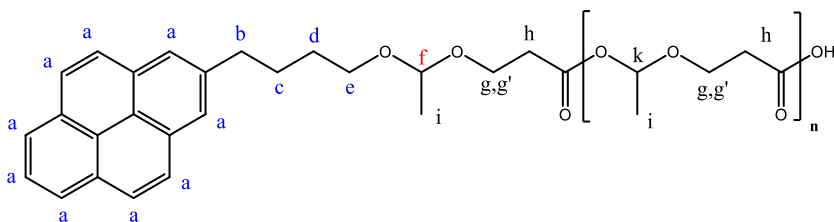


Figure S 5: <sup>1</sup>H-NMR (400 MHz) analysis of poly(2-methyl-1,3-dioxan-4-one) (P(MDO)) in CDCl<sub>3</sub> referenced to the pyrene end group (polymerized at room temperature). All signals are in agreement with published spectra of P(MDO).<sup>14,15</sup> The proton belonging to the pyrene butanol end group marked as “e” was assigned based on the <sup>1</sup>H-derived COSY measurement shown in Figure S 7. The chemical shift of the acetal proton marked as f (pyrene-(CH<sub>2</sub>)<sub>4</sub>-CH(CH<sub>3</sub>)-O-) is in accordance to spectra of P(MDO) initiated by 3-phenyl-1-propanol, but is covered partially by the resonance signal of the cyclic product.<sup>15</sup> Further analysis, such as MALDI and SEC analysis supported the incorporation of pyrene butanol as end group (Figure S 11, Figure S 12). The chemical shift of the resonance signal y, belonging to a polyester unit, is comparable to those reported for poly(3-hydroxypropionic ester). All assignments are further supported by COSY-NMR (Figure S 7).

## <sup>1</sup>H-NMR of poly(pyrene butanol-MDO) synthesized at 0°C

Molecular structure of P(MDO):



Molecular structure of P(MDO) with incorporation of polyester units:

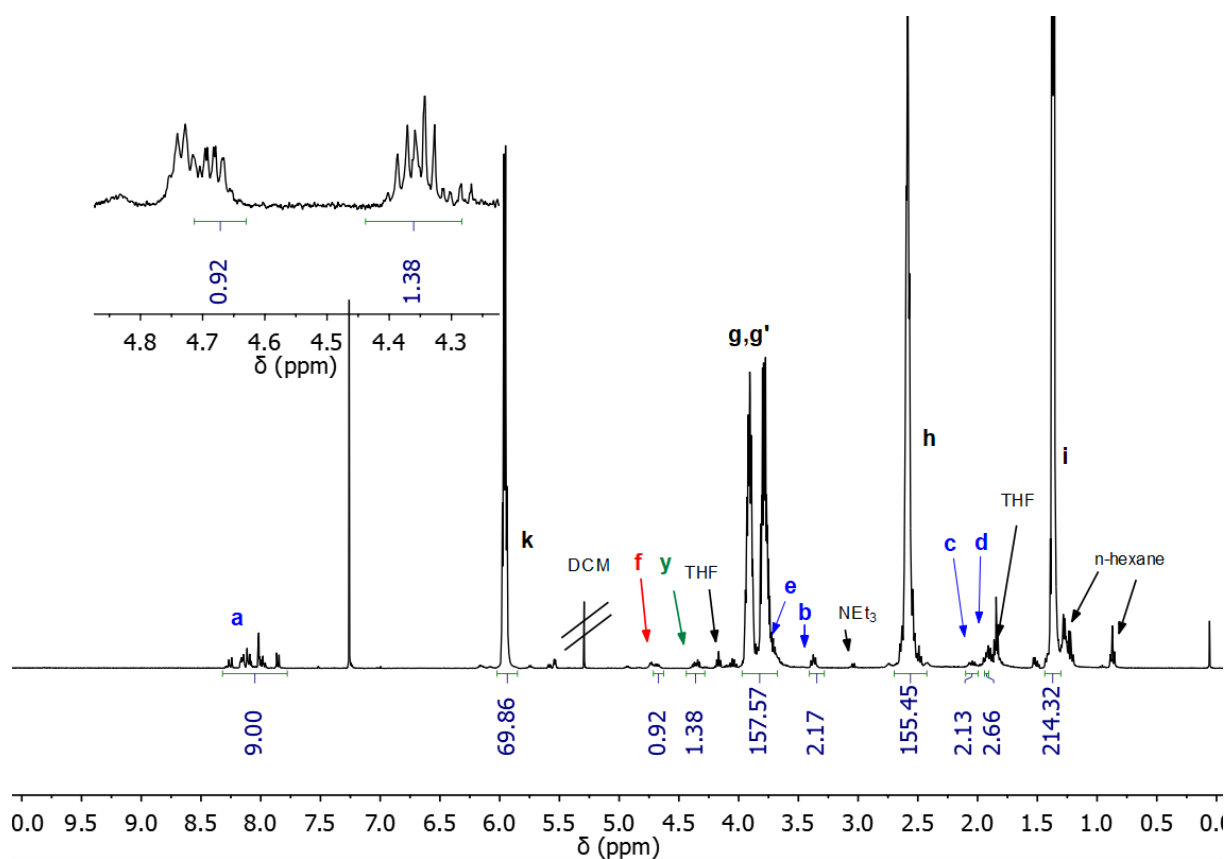
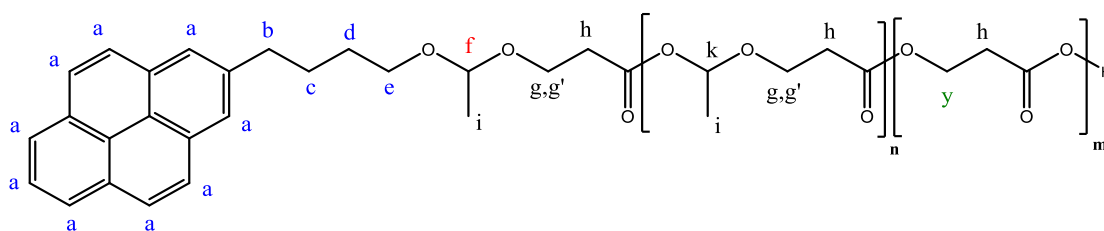
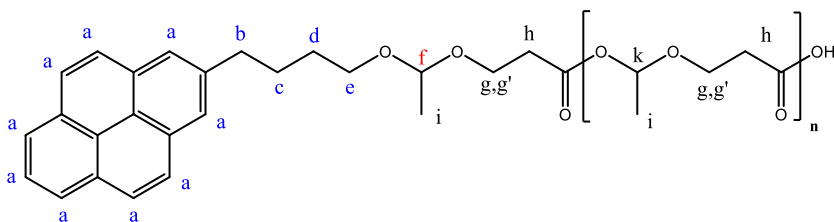


Figure S 6: <sup>1</sup>H-NMR(400 MHz) analysis of poly(2-methyl-1,3-dioxan-4-one) (P(MDO)) in CDCl<sub>3</sub> referenced to its pyrene end group (polymerized at 0°C). The assignment of the resonance signals is in analogy to Figure S 5. In contrast to the polymerisation at room temperature slightly less cyclic side product is observed and, therefore, the acetal proton resonance f (pyrene-(CH<sub>2</sub>)<sub>4</sub>-CH(CH<sub>3</sub>)-O-) becomes more visible.

## $^1\text{H}$ , $^1\text{H}$ -COSY NMR of poly(pyrene butanol-MDO)

Molecular structure of  $P(\text{MDO})$ :



Molecular structure of  $P(\text{MDO})$  with incorporation of polyester units:

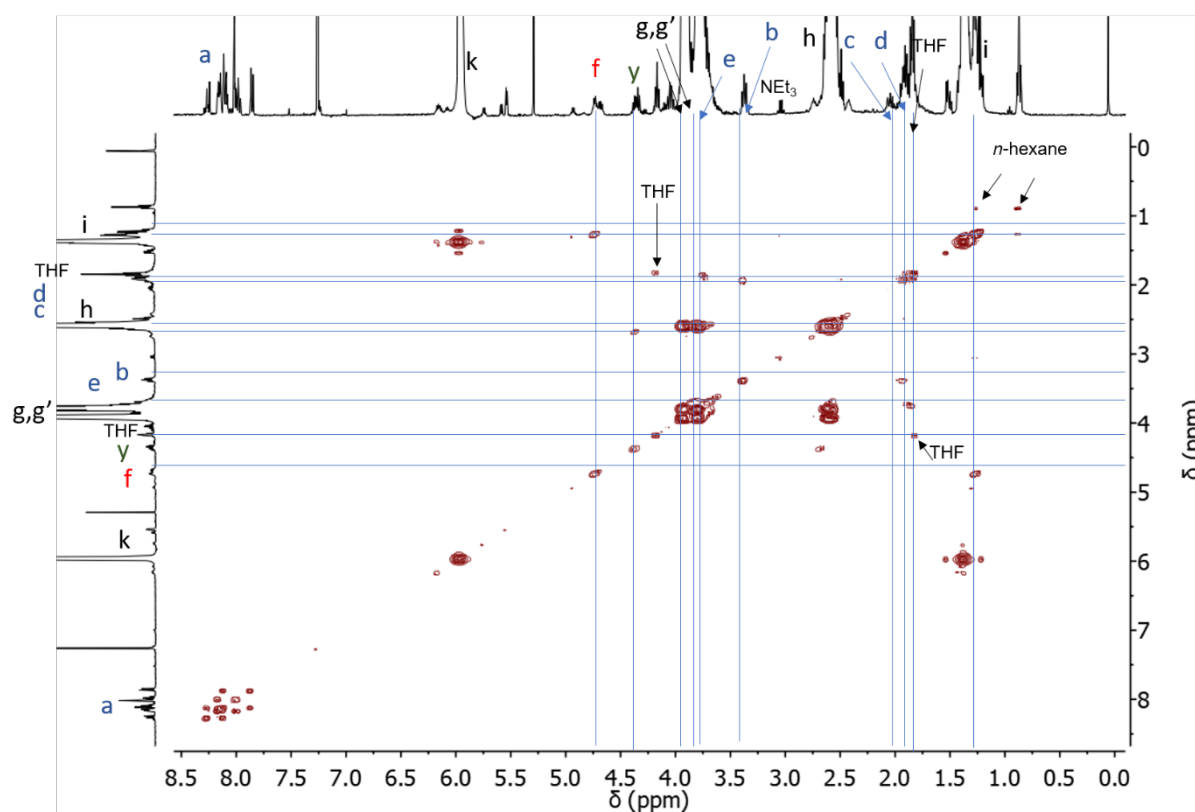
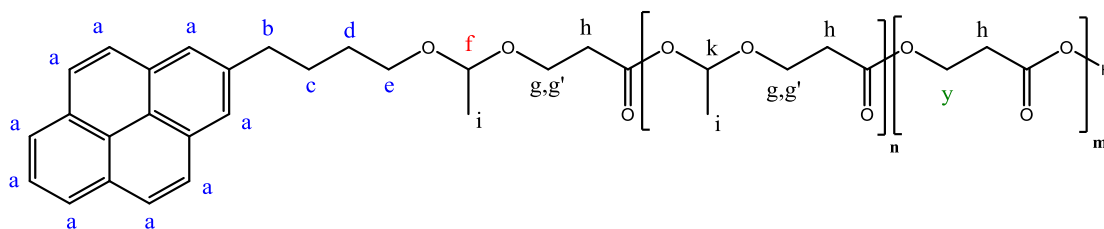


Figure S 7: COSY-NMR analysis of poly(2-methyl-1,3-dioxan-4-one) ( $P(\text{MDO})$ ) in  $\text{CDCl}_3$ . COSY-NMR unmasks all signals corresponding to the pyrene butanol end group. Further, the coupling of the acetal proton  $f$  and the proton corresponding to the ester unit are in agreement with their assignments.

### $^{13}\text{C}$ -NMR of poly(pyrene butanol-MDO)

Molecular structure of P(MDO):

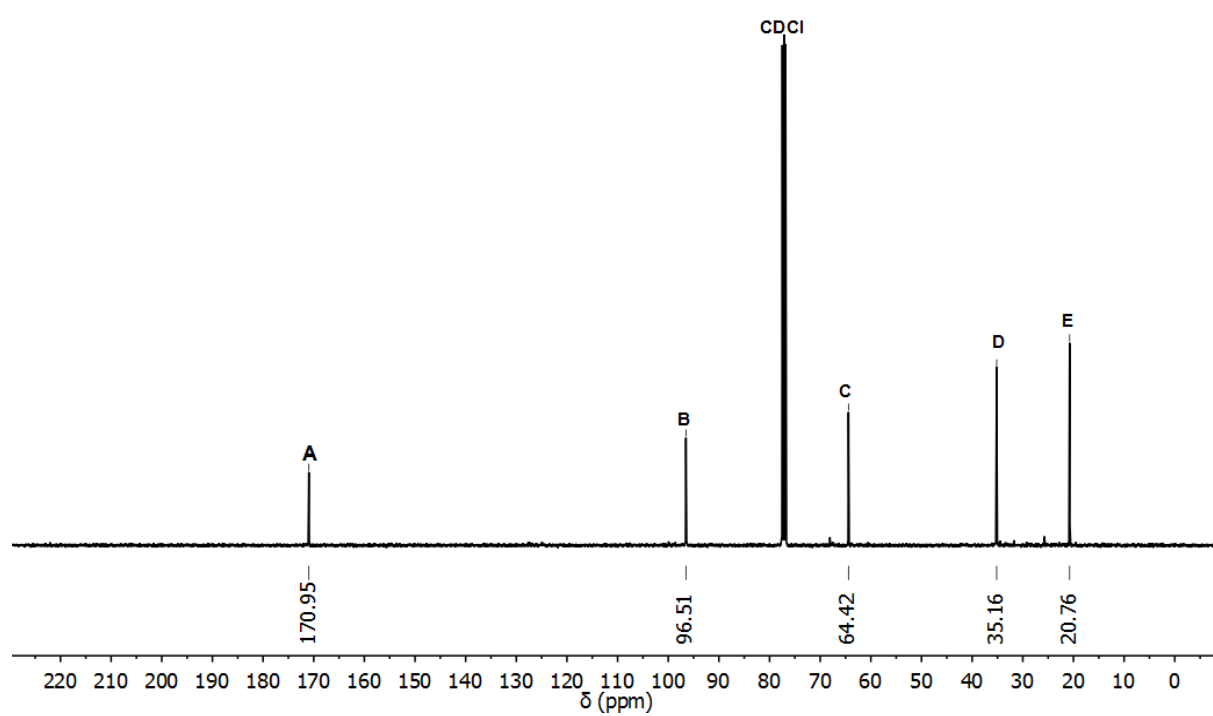
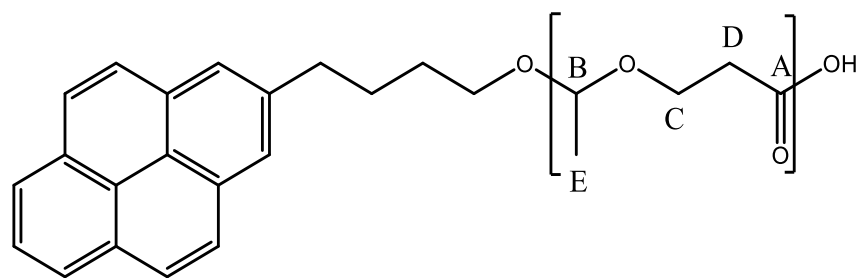


Figure S 8:  $^{13}\text{C}$ -NMR (100 MHz) of P(MDO) in  $\text{CDCl}_3$ .

**$^1\text{H}$ ,  $^{13}\text{C}$ -HSQC NMR of poly(pyrene butanol-MDO)**

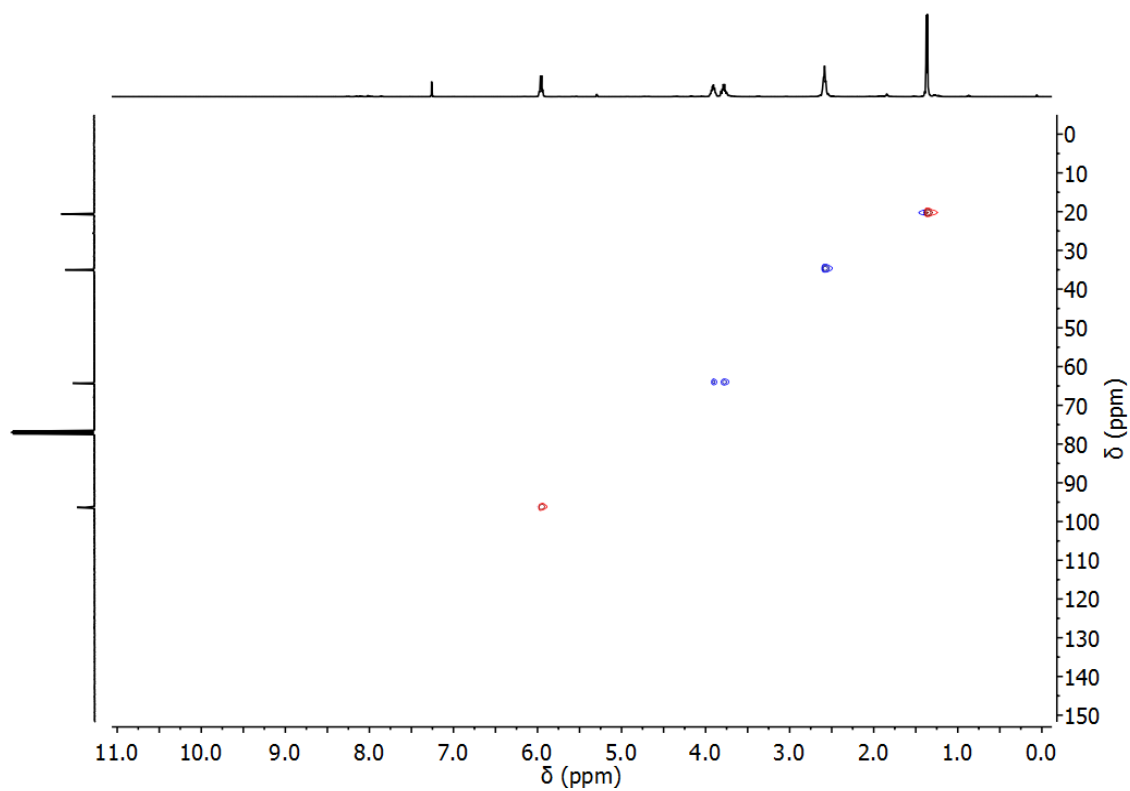


Figure S 9: HSQC NMR analysis of P(MDO) in  $\text{CDCl}_3$ .

**$^1\text{H}$ ,  $^{13}\text{C}$ -HMBC NMR of poly(pyrene butanol-MDO)**

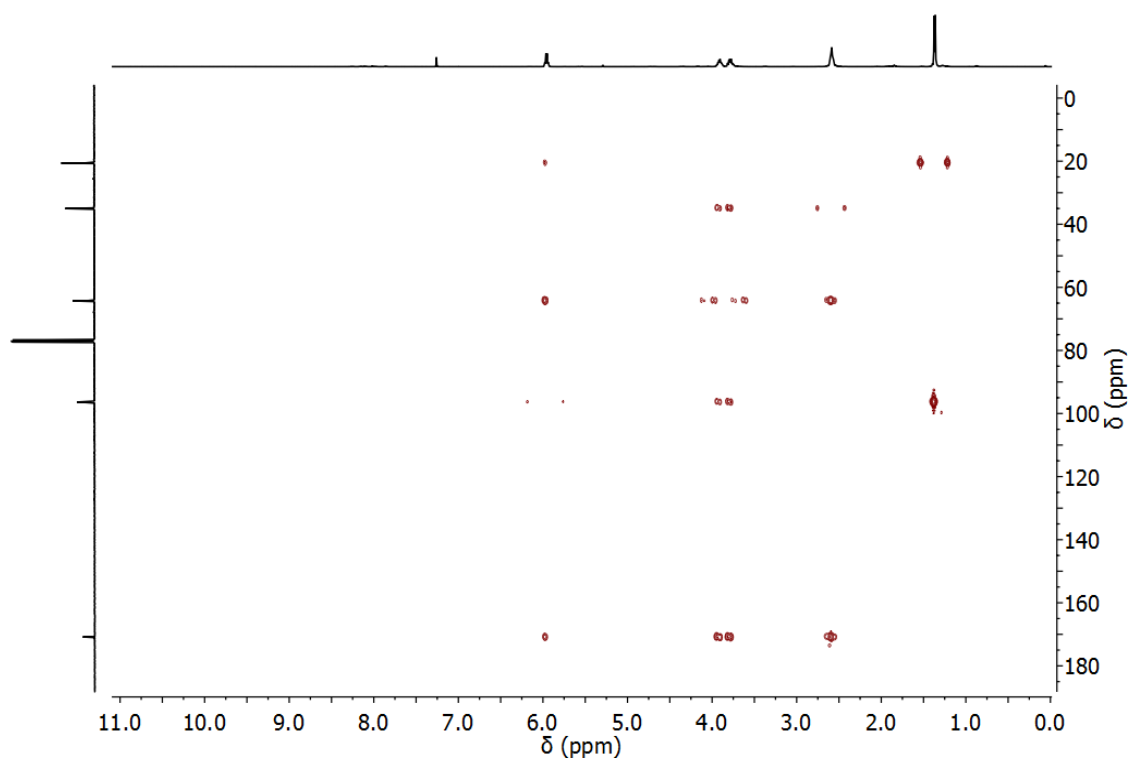
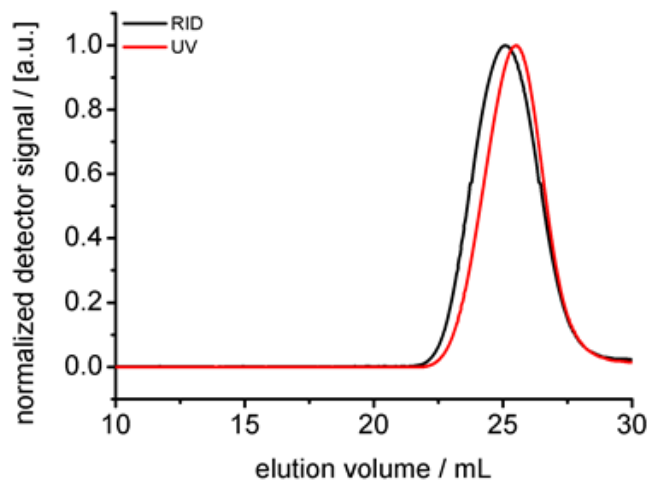


Figure S 10: HMBC NMR analysis of P(MDO) in  $\text{CDCl}_3$ .

## SEC of poly(pyrene butanol-MDO)

A: Polymerisation at room temperature



B: Polymerisation at 0°C

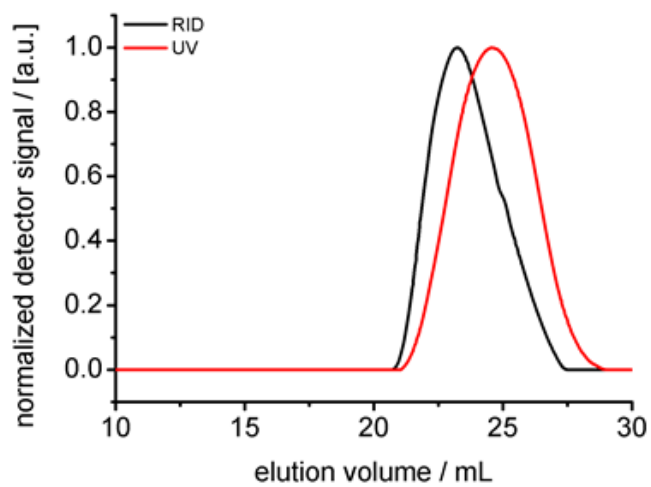
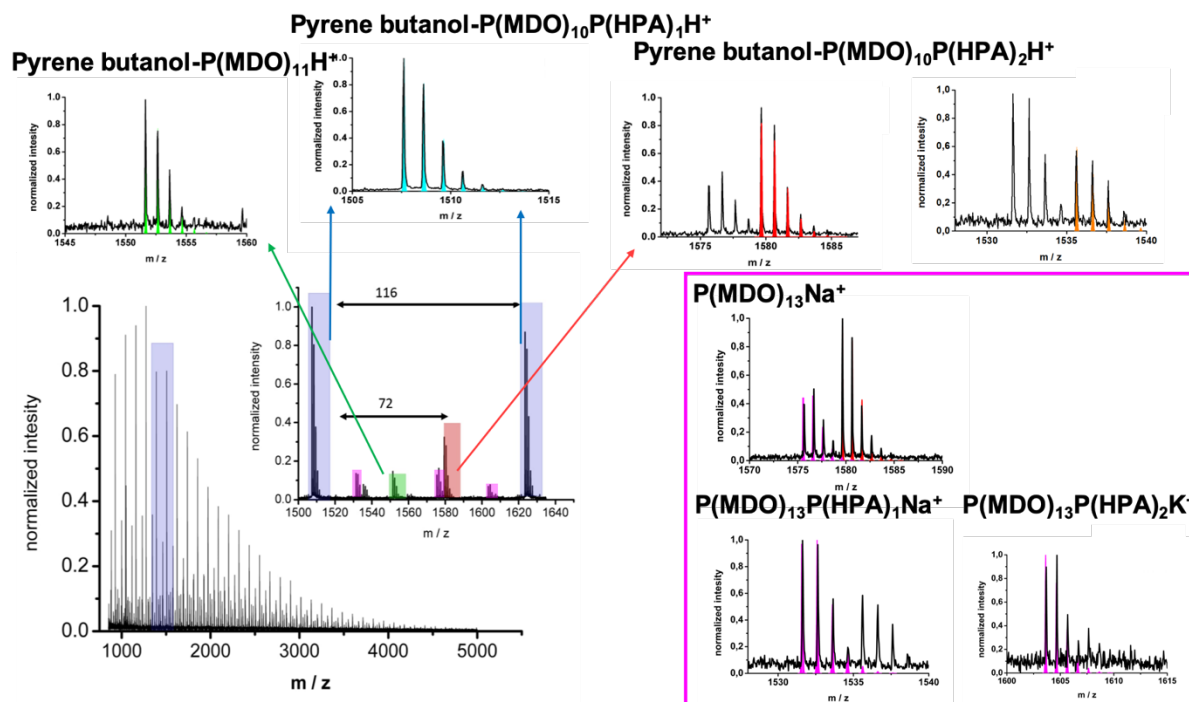


Figure S 11: THF SEC trace of P(MDO) detected by refractive index (black) and (UV) (red). Note that the incorporation of the pyrene butanol end group affords a strong UV signal.

## MALDI-ToF MS of poly(pyrene butanol-MDO)

A:



B:

		Empirical formula
<span style="display:inline-block; width:15px; height:15px; background-color:lightblue;"></span>	Pyrene butanol-P(MDO) <sub>10</sub> P(HPA) <sub>1</sub> H <sup>+</sup>	C <sub>73</sub> H <sub>102</sub> O <sub>33</sub> H <sup>+</sup>
<span style="display:inline-block; width:15px; height:15px; background-color:lightgreen;"></span>	Pyrene butanol-P(MDO) <sub>11</sub> H <sup>+</sup>	C <sub>75</sub> H <sub>106</sub> O <sub>34</sub> H <sup>+</sup>
<span style="display:inline-block; width:15px; height:15px; background-color:lightcoral;"></span>	Pyrene butanol-P(MDO) <sub>10</sub> P(HPA) <sub>2</sub> H <sup>+</sup>	C <sub>76</sub> H <sub>106</sub> O <sub>35</sub> H <sup>+</sup>
<span style="display:inline-block; width:15px; height:15px; background-color:lightpurple;"></span>	P(MDO) <sub>13</sub> Na <sup>+</sup> P(MDO) <sub>13</sub> P(HPA) <sub>1</sub> Na <sup>+</sup> P(MDO) <sub>13</sub> P(HPA) <sub>2</sub> K <sup>+</sup>	C <sub>65</sub> H <sub>104</sub> O <sub>39</sub> Na <sup>+</sup> C <sub>68</sub> H <sub>108</sub> O <sub>41</sub> Na <sup>+</sup> C <sub>71</sub> H <sub>112</sub> O <sub>43</sub> K <sup>+</sup>

Figure S 12: MALDI-spectra of pyrene butanol initiated P(MDO) - overlay of simulated mass spectra (coloured) and measured data (black). Mass peaks marked in blue, green and red match to simulated mass peaks corresponding to P(MDO) with pyrene butanol endgroup. Peaks shown in light purple correspond to cyclic homopolymers without a pyrene butanol end group.

## Analytical data of mPEG<sub>48</sub>-*b*-poly(MDO) block copolymers:

All <sup>1</sup>H-NMR spectra from block copolymers are referenced to the ethylene glycol units of polyethylene glycol methyl ether. Previously, the average number of ethylene glycol units was determined to be 194 per chain via <sup>1</sup>H NMR of pure mPEG in CDCl<sub>3</sub> referenced to its methyl end group (Figure S 13). Therefore, the degree of polymerisation of block copolymers could be determined based on the integral of the poly(esteracetal) groups referenced to the ethylene glycol units of mPEG. To consider the different chemical shift of the first acetal proton one proton was added to the integral of the polyesteracetal for calculating the exact degree of polymerisation for the poly(MDO)-block.

### <sup>1</sup>H-NMR of mPEG

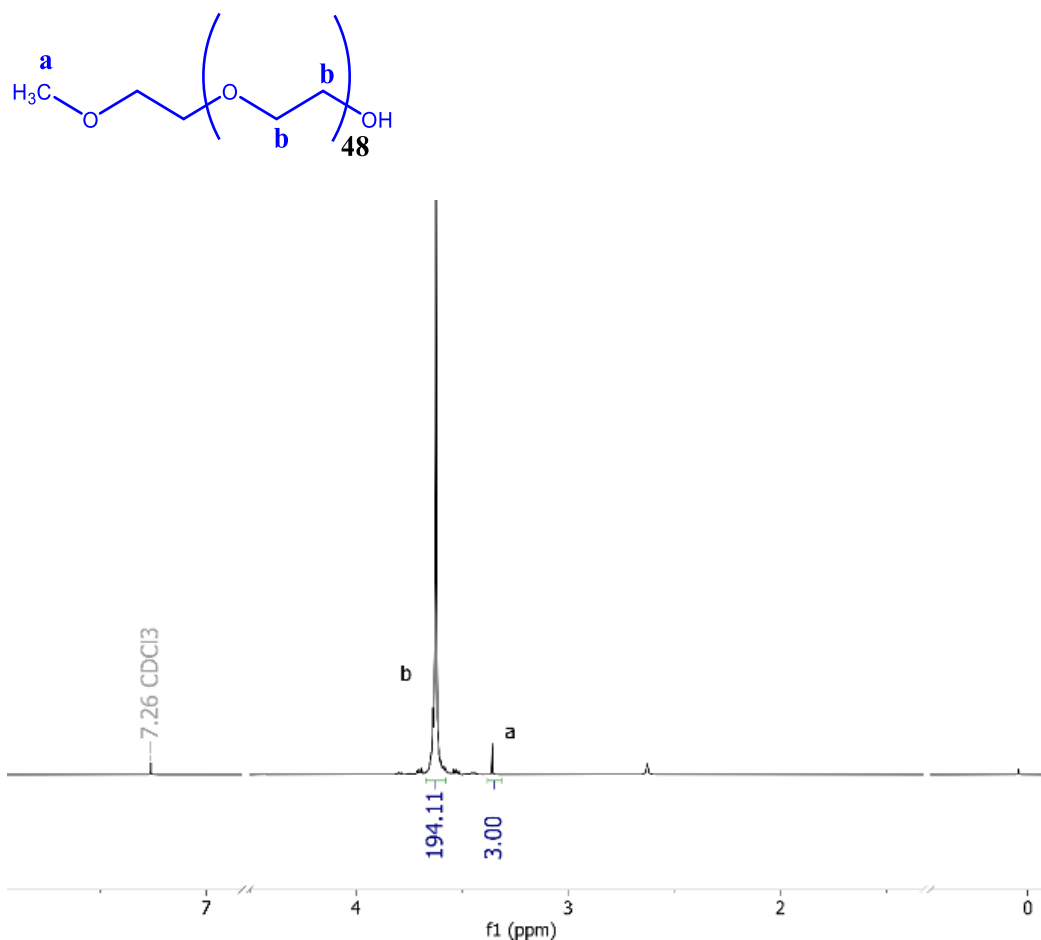


Figure S 13: mPEG<sub>48</sub> as macro-initiator for the ring opening polymerization of MDO. The determined integral of the ethylene glycol units in relation to the methyl ether group has been used as reference for determining the degree of polymerization of mPEG<sub>48</sub>-*b*-P(MDO) block copolymers.

### Assignment of the proton resonance signals:

All assigned proton peaks are in conformity with spectra from literature.<sup>16</sup> The acetal proton (mPEG-O-CH(CH<sub>3</sub>)-O-) appears at 4.77, which is in good agreement with published spectra for P(MDO) initiated by 2-hydroxyethyl methacrylate.<sup>16</sup> <sup>1</sup>H-NMR derived COSY analysis revealed a coupling with two doublets at 1.30 and 1.28 ppm with a coupling constant similar as the esteracetal quartet (-O-CH(CH<sub>3</sub>)-O-) at 5.96 ppm to the doublet (-O-CH(CH<sub>3</sub>)-O-) at 1.37 ppm.

In order to estimate the degree of polymerisation for the MDO block, the sum of the integrals of the poly(esteracetal) protons at 5.96 ppm and the single acetal proton at 4.77 could be used. This is in accordance to the polymer signals of the two polymeric methylene units or the sum of the methyl protons of the polymeric esteracetal and single acetal group, respectively.

### <sup>1</sup>H-NMR of mPEG<sub>48</sub>-b-P(MDO)<sub>15</sub>

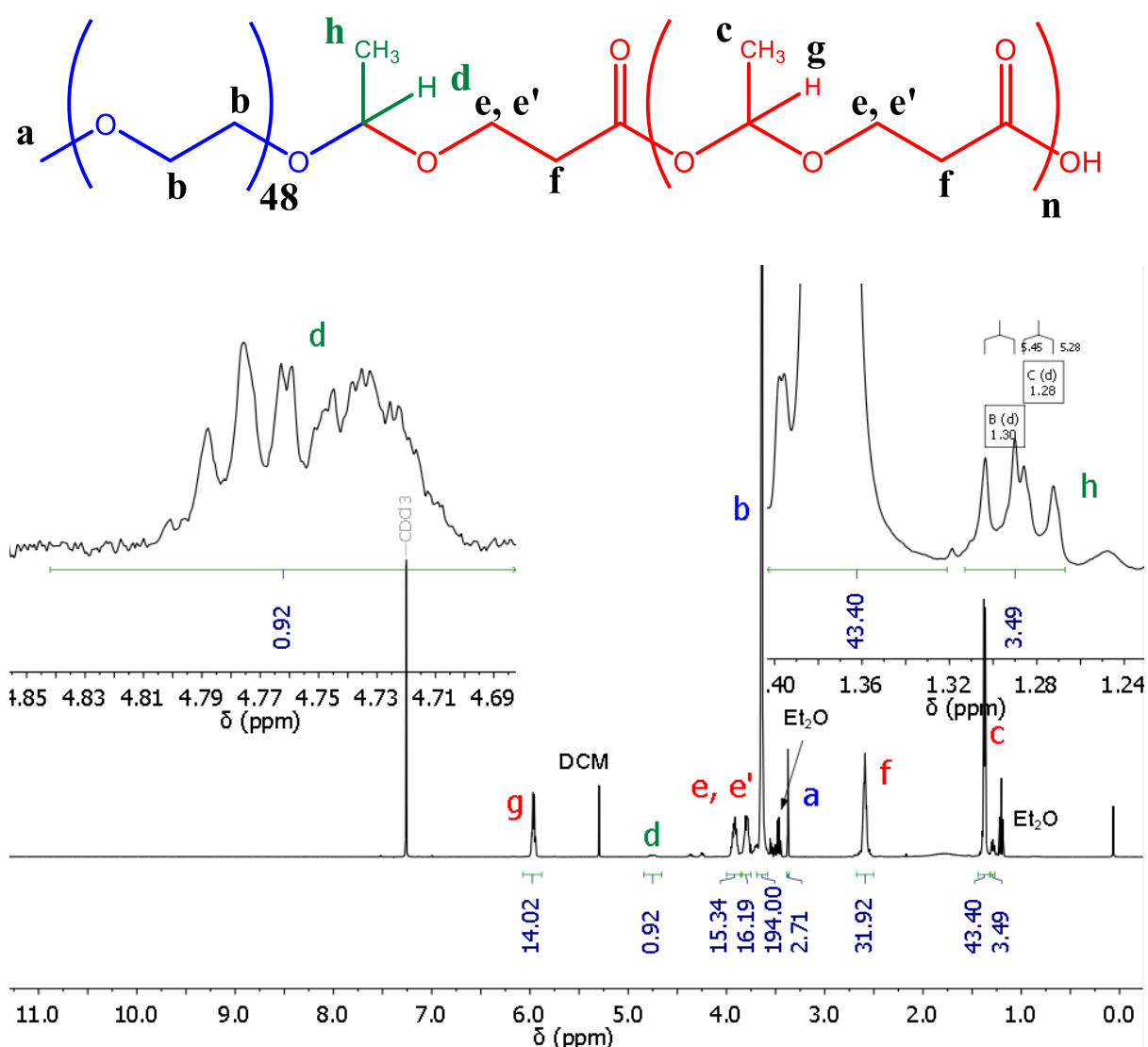


Figure S 14: <sup>1</sup>H NMR (400 MHz) mPEG<sub>48</sub>-b-P(MDO)<sub>15</sub> in CDCl<sub>3</sub>.

### MALDI-ToF MS of mPEG<sub>48</sub> and mPEG<sub>48</sub>-b-P(MDO)<sub>15</sub>

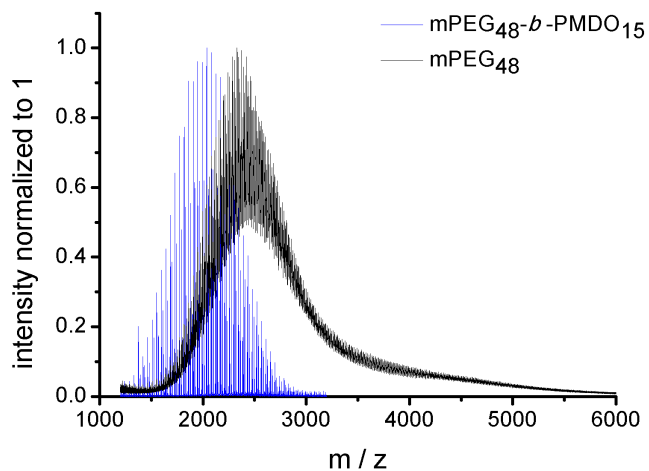


Figure S 15: MALDI spectra of mPEG<sub>48</sub>-b-P(MDO)<sub>15</sub> in black. The macro-initiator mPEG<sub>48</sub> is shown in blue colour.

### SEC of mPEG<sub>48</sub> and mPEG<sub>48</sub>-b-P(MDO)<sub>15</sub>

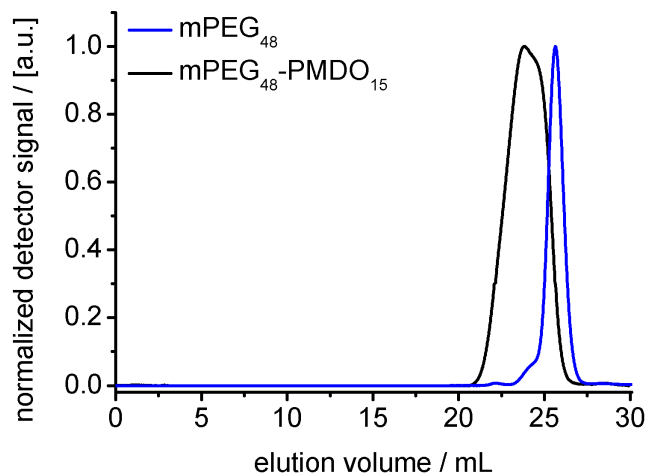


Figure S 16: THF SEC elugrams of mPEG<sub>48</sub>-b-P(MDO)<sub>15</sub> block copolymers (black) and mPEG<sub>48</sub> (blue) recorded by RI detector.  $D = 1.46$ .

### $^1\text{H-NMR}$ of $\text{mPEG}_{48}\text{-b-P(MDO)}_{23}$

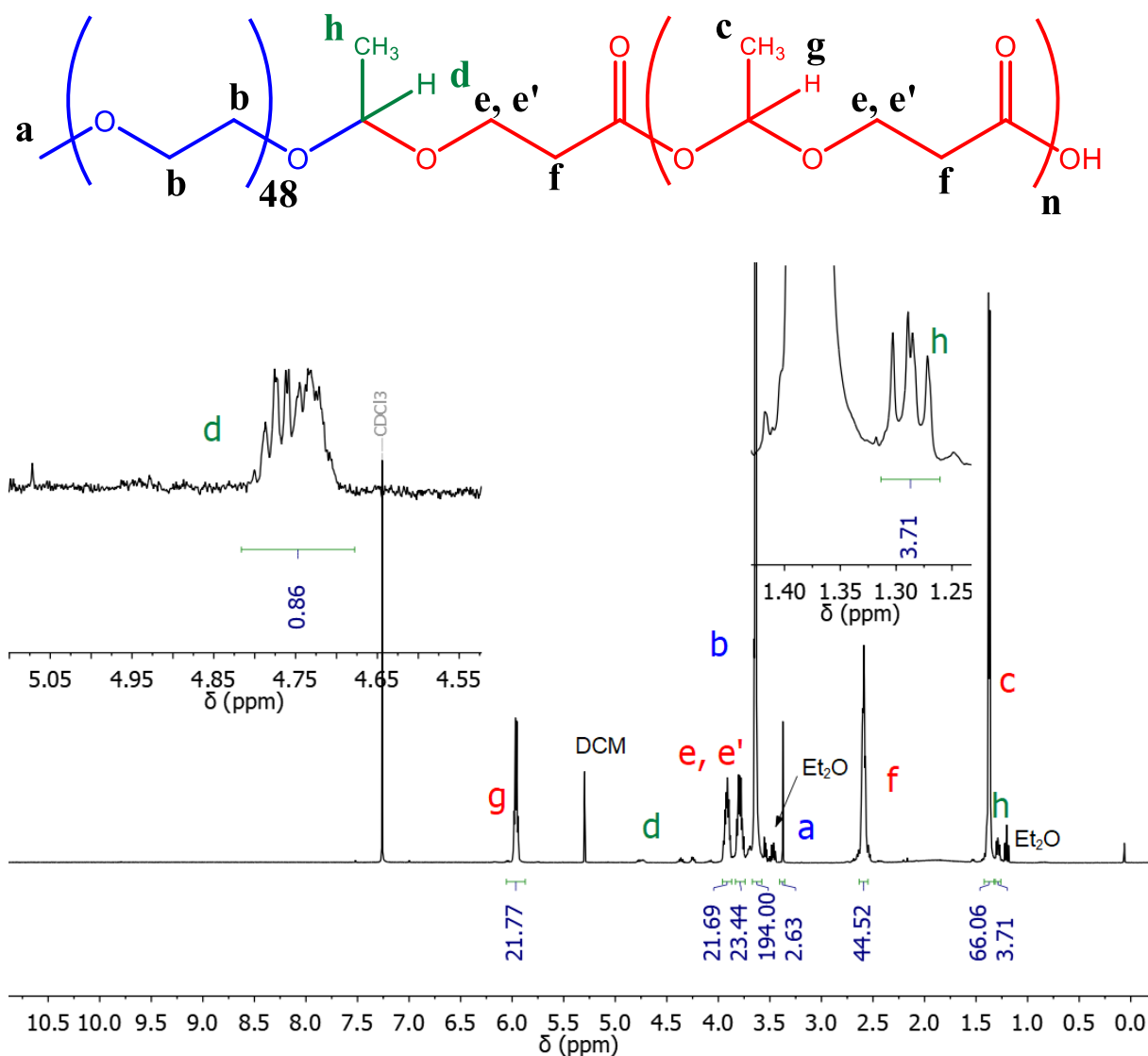


Figure S 17:  $^1\text{H-NMR}$  analysis (400 MHz) of  $\text{mPEG}_{48}\text{-b-P(MDO)}_{23}$  in  $\text{CDCl}_3$ .

### MALDI-ToF MS of mPEG<sub>48</sub> and mPEG<sub>48</sub>-b-P(MDO)<sub>23</sub>

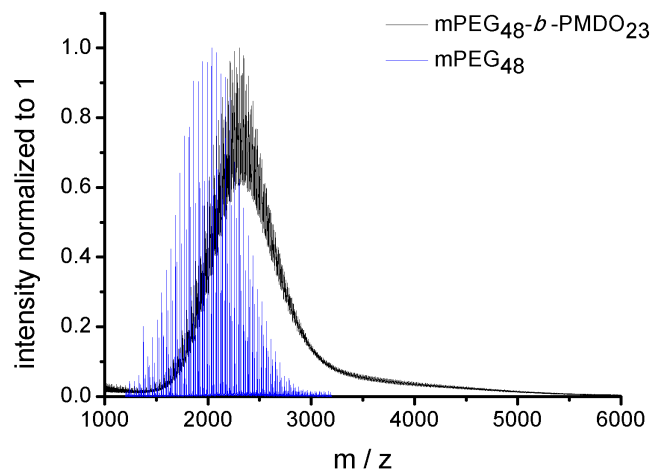


Figure S 18: MALDI spectra of mPEG<sub>48</sub>-b-P(MDO)<sub>23</sub> in black. The macro-initiator mPEG<sub>48</sub> is shown in blue colour.

### SEC of mPEG<sub>48</sub> and mPEG<sub>48</sub>-b-P(MDO)<sub>23</sub>

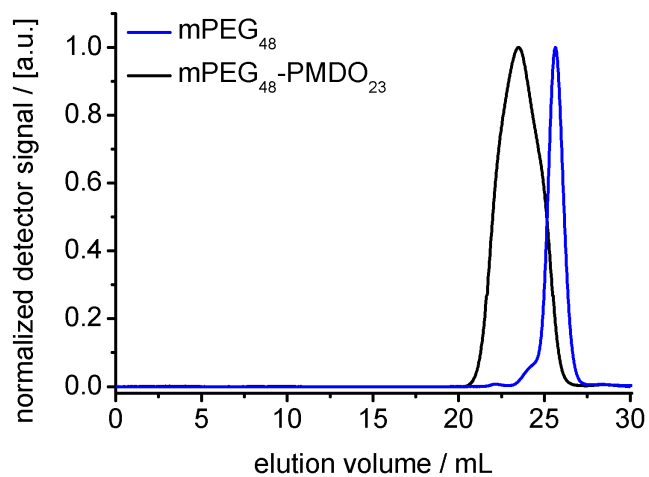


Figure S 19: THF SEC elugrams of mPEG<sub>48</sub>-b-P(MDO)<sub>23</sub> block copolymers (black) and mPEG<sub>48</sub> (blue) recorded by RI detector.  $D = 1.57$ .

### $^1\text{H-NMR}$ of $\text{mPEG}_{48}\text{-b-P(MDO)}_{50}$

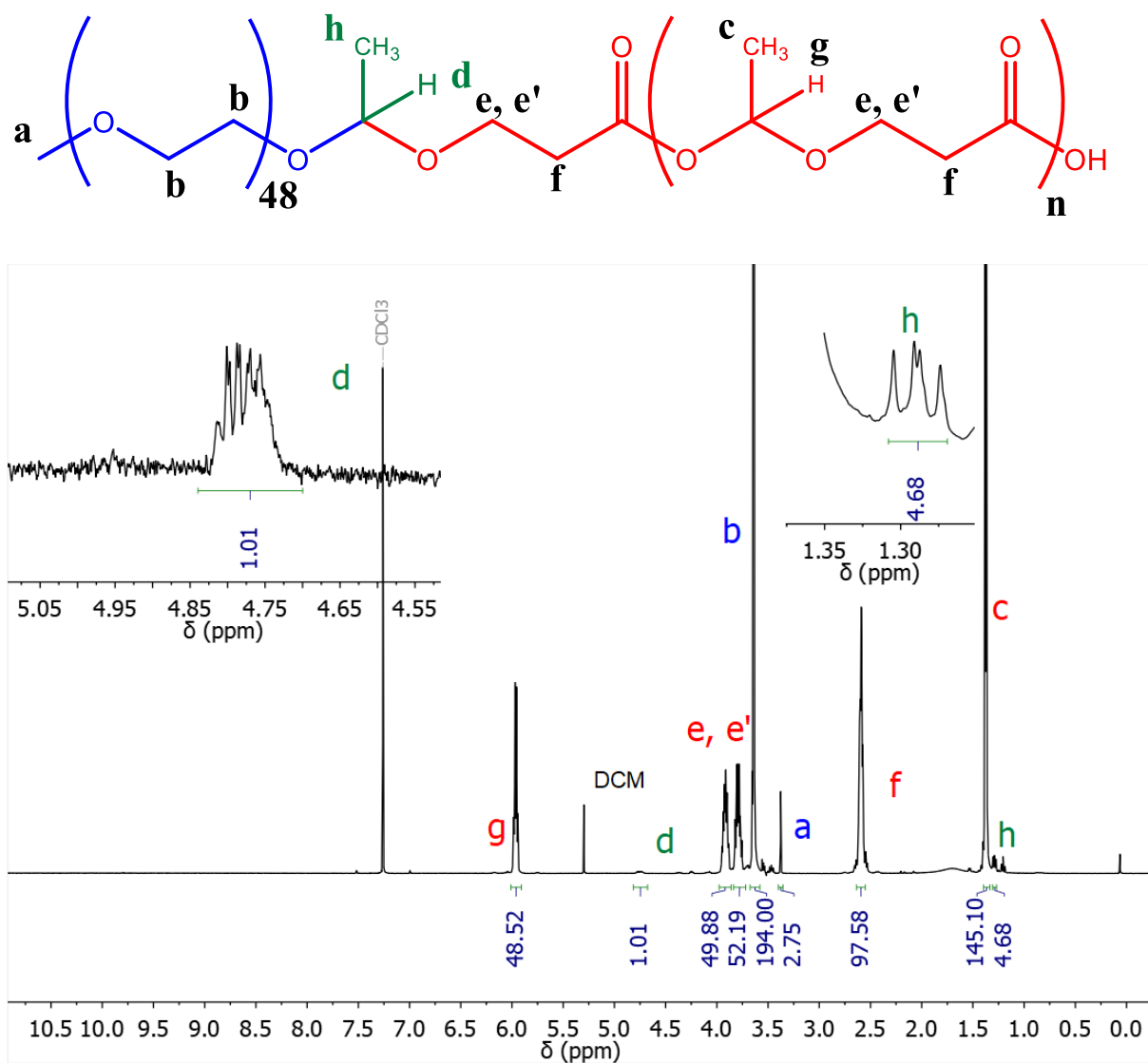


Figure S 20:  $^1\text{H-NMR}$  analysis (400 MHz) of  $\text{mPEG}_{48}\text{-b-P(MDO)}_{50}$  in  $\text{CDCl}_3$ .

### MALDI-ToF MS of mPEG<sub>48</sub> and mPEG<sub>48</sub>-b-P(MDO)<sub>50</sub>

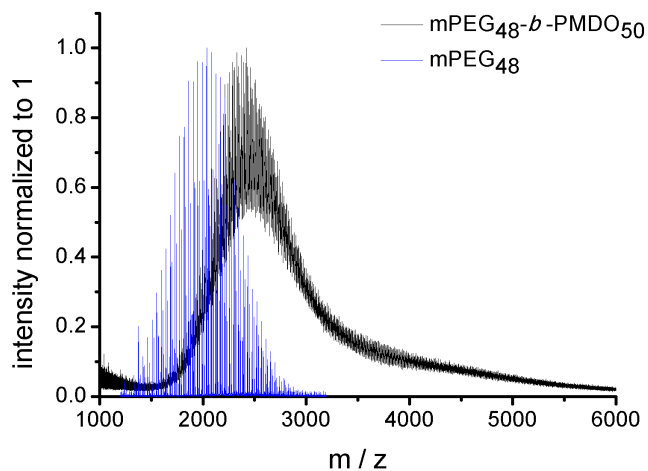


Figure S 21: MALDI spectra of mPEG<sub>48</sub>-b-P(MDO)<sub>50</sub> in black. The macro-initiator mPEG<sub>48</sub> is shown in blue colour.

### SEC of mPEG<sub>48</sub> and mPEG<sub>48</sub>-b-P(MDO)<sub>50</sub>

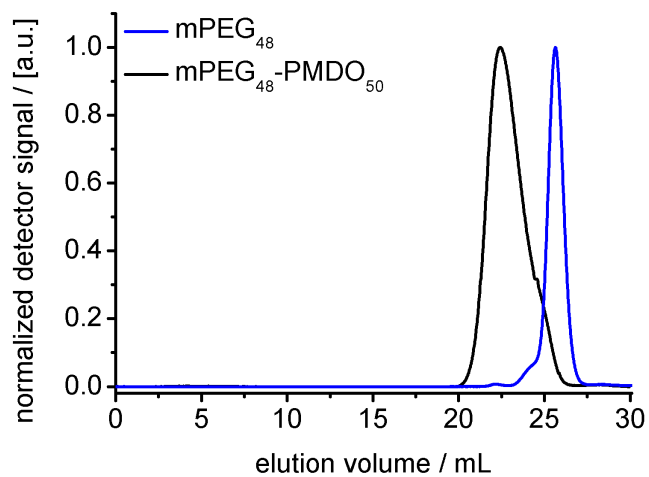


Figure S 22: THF SEC elugrams of mPEG<sub>48</sub>-b-P(MDO)<sub>50</sub> block copolymers (black) and mPEG<sub>48</sub> (blue) recorded by RI detector.  $D = 1.65$

### $^1\text{H-NMR}$ of mPEG<sub>48</sub>-b-P(MDO)<sub>71</sub>

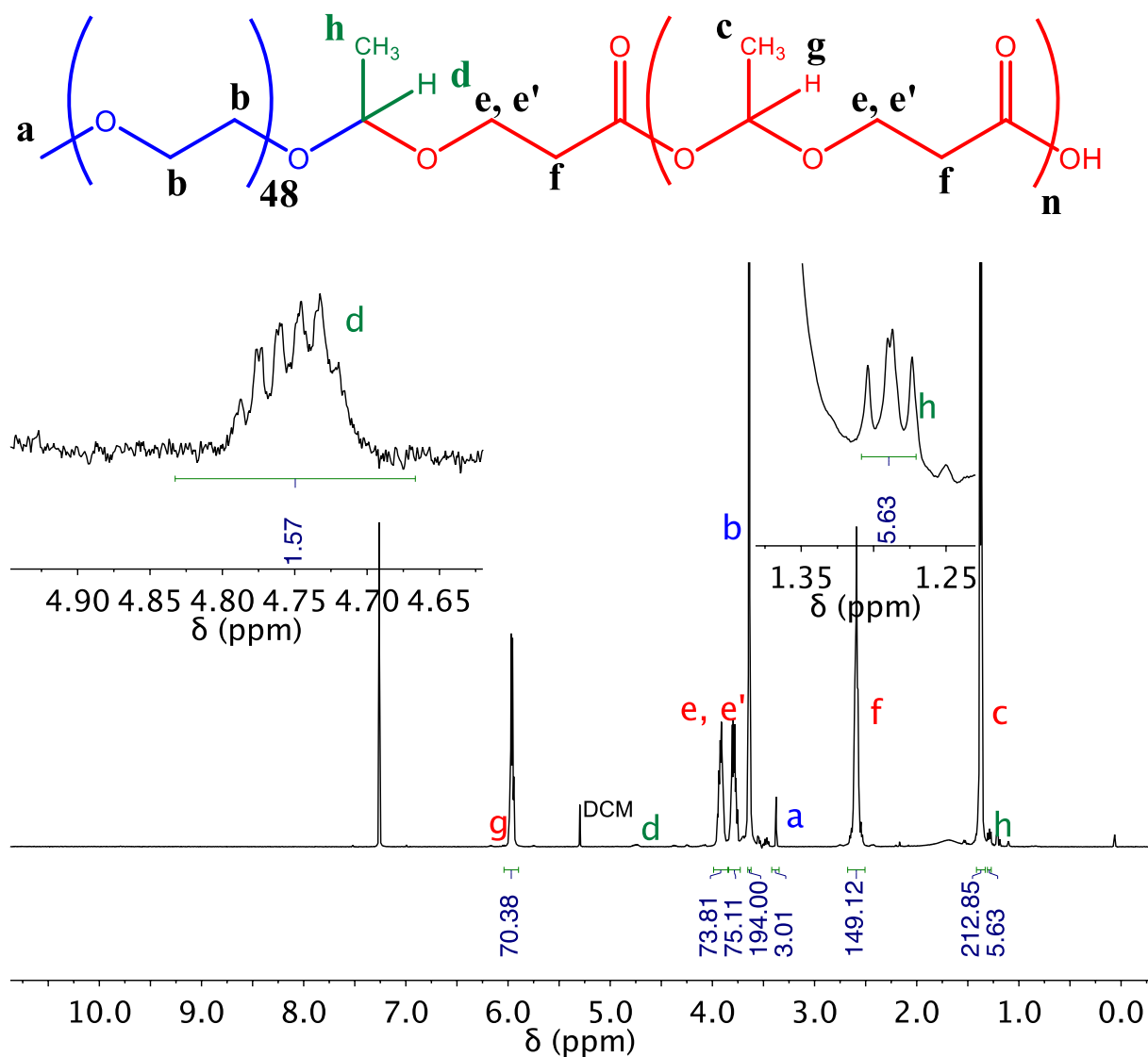


Figure S 23:  $^1\text{H-NMR}$  analysis (400 MHz) of mPEG<sub>48</sub>-b-poly(MDO)<sub>71</sub> in  $\text{CDCl}_3$ .

### MALDI-ToF MS of mPEG<sub>48</sub> and mPEG<sub>48</sub>-b-P(MDO)<sub>71</sub>

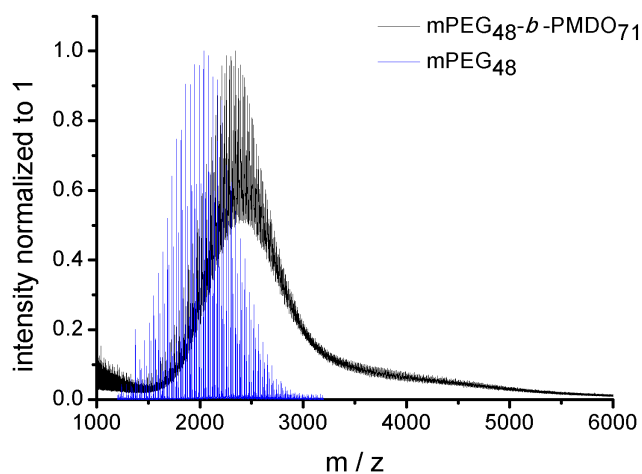


Figure S 24: MALDI spectra mPEG<sub>48</sub>-b-P(MDO)<sub>71</sub> in black. The macro-initiator mPEG<sub>48</sub> is shown in blue colour.

### SEC of mPEG<sub>48</sub> and mPEG<sub>48</sub>-b-P(MDO)<sub>71</sub>

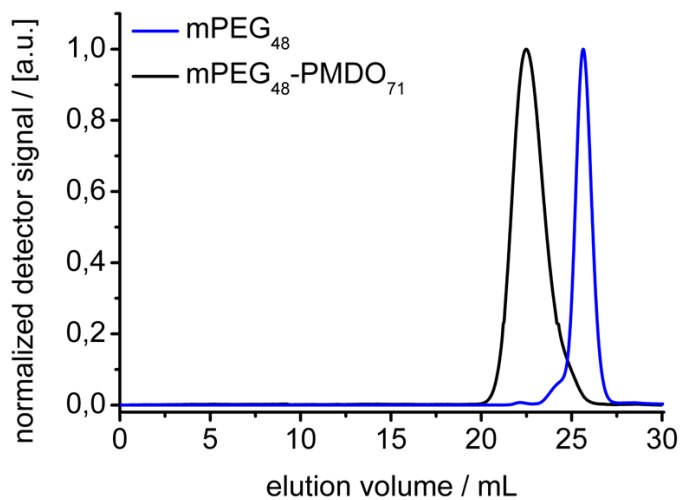


Figure S 25: THF SEC elugrams of mPEG<sub>48</sub>-b-P(MDO)<sub>71</sub> block copolymers (black) and mPEG<sub>48</sub> (blue) recorded by RI detector.  $D = 1.48$ .

**$^1\text{H}$ ,  $^1\text{H}$ -COSY NMR of mPEG<sub>48</sub>-b-P(MDO)<sub>71</sub>**

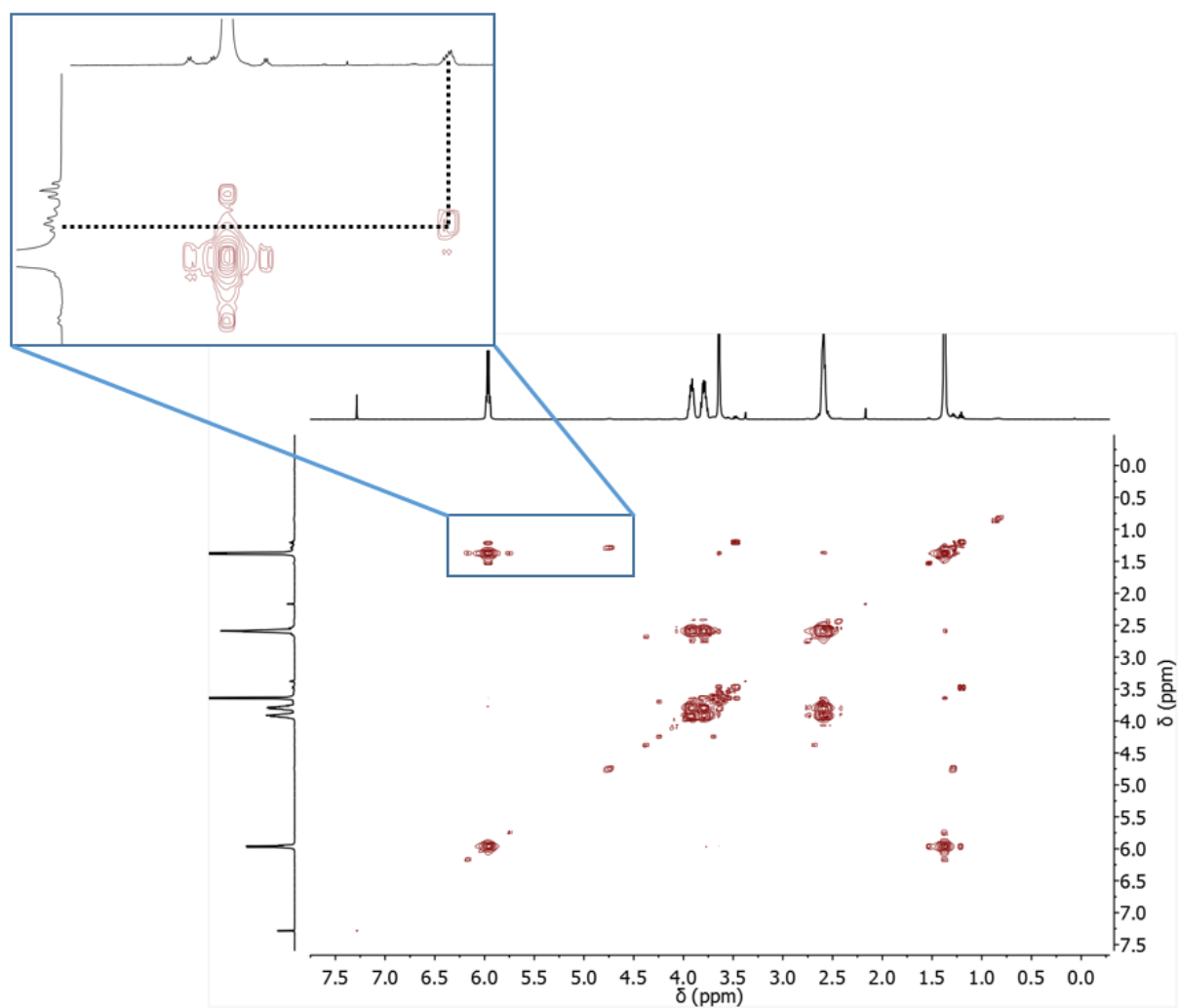


Figure S 26:  $^1\text{H}$ -NMR derived COSY spectra of mPEG<sub>48</sub>-b-P(MDO)<sub>71</sub> in  $\text{CDCl}_3$ . The zoomed area shows the coupling between the acetal proton ( $-\text{O}-\text{CH}(\text{CH}_3)-\text{O}-$ ) and the methyl protons ( $-\text{O}-\text{CH}(\text{CH}_3)-\text{O}-$ ).

**$^{13}\text{C}$ -NMR of poly(pyrene mPEG<sub>48</sub>-b-P(MDO)<sub>71</sub>)**

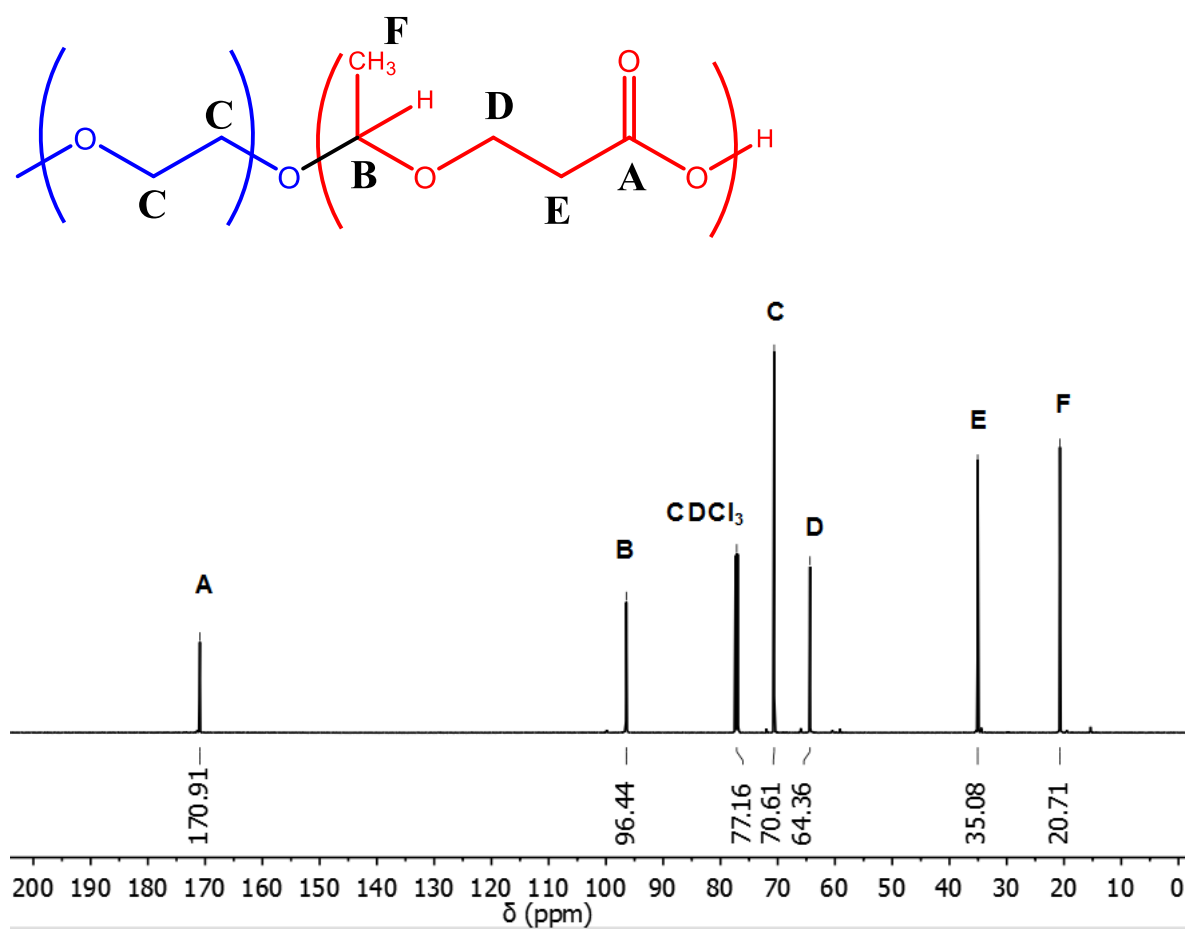


Figure S 27:  $^{13}\text{C}$ -NMR NMR analysis (150 MHz) of mPEG<sub>48</sub>-b-P(MDO)<sub>71</sub> in  $\text{CDCl}_3$ .

**$^1\text{H}$ ,  $^{13}\text{C}$ -HSQC NMR of mPEG<sub>48</sub>-b-P(MDO)<sub>71</sub>**

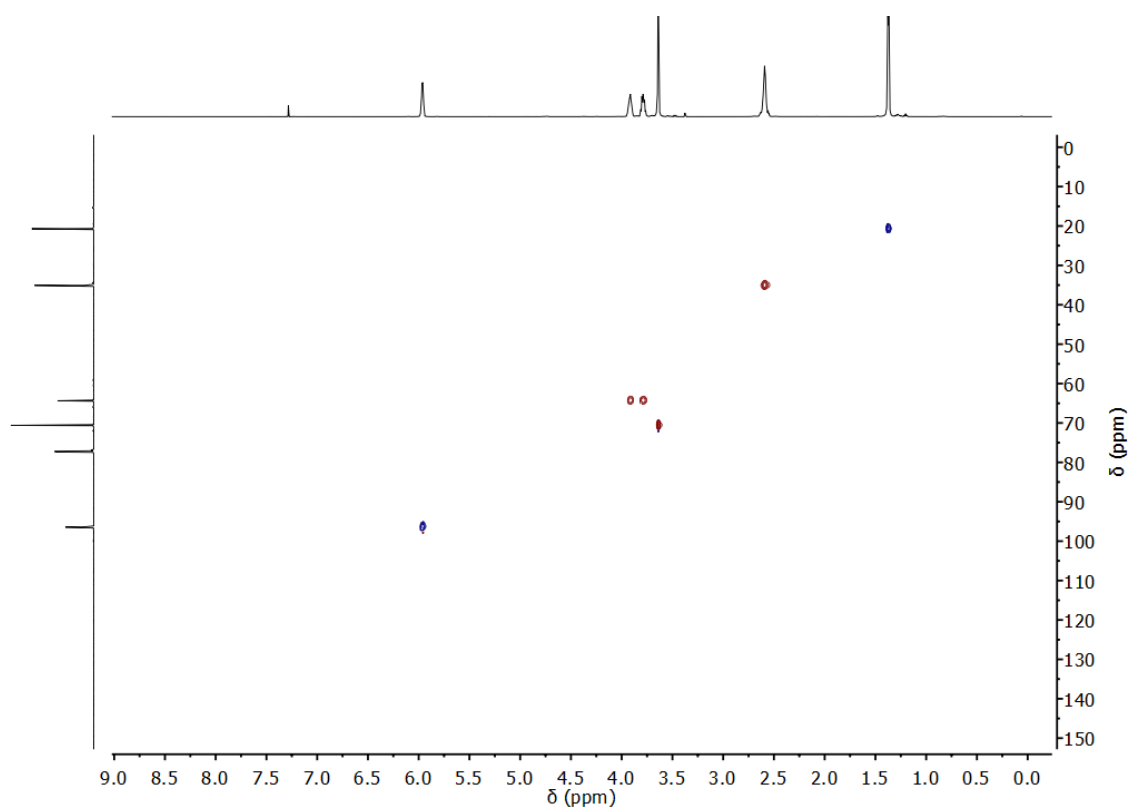


Figure S 28: HSQC-NMR analysis of mPEG<sub>48</sub>-b-P(MDO)<sub>71</sub> in CDCl<sub>3</sub>.

**$^1\text{H}$ ,  $^{13}\text{C}$ -HMBC NMR of mPEG<sub>48</sub>-b-P(MDO)<sub>71</sub>**

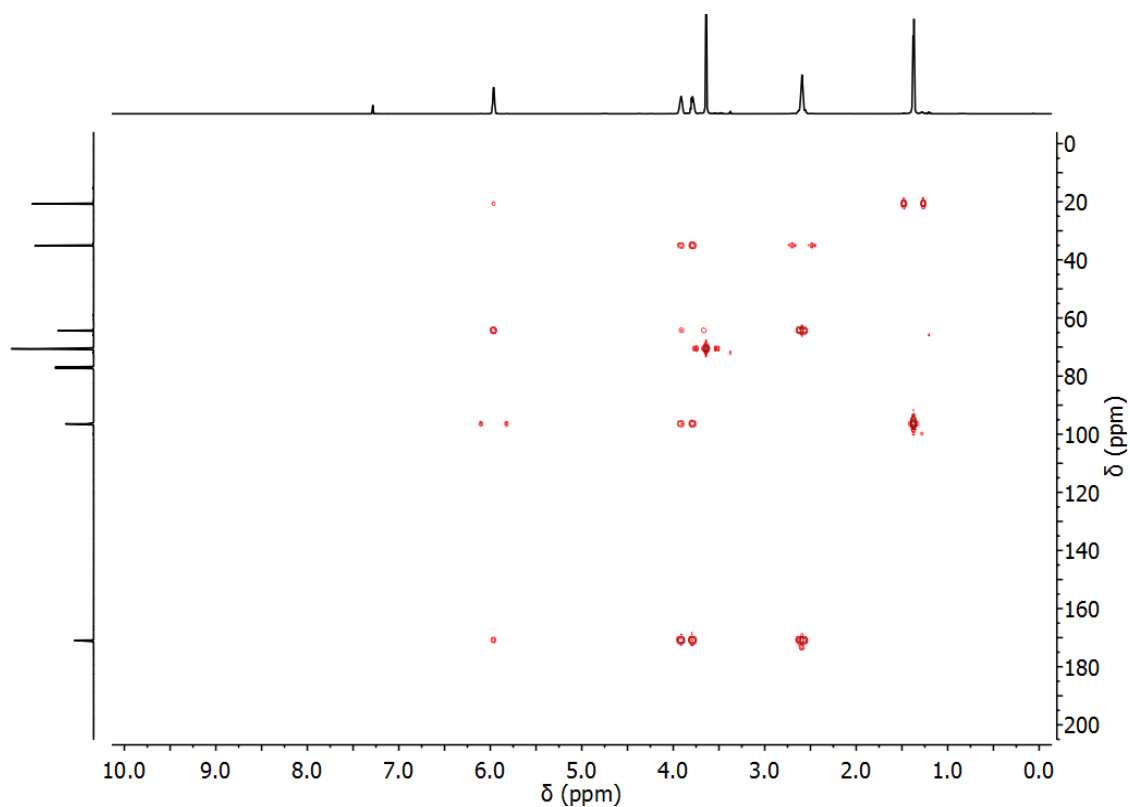


Figure S 29: HMBC-NMR analysis of mPEG<sub>48</sub>-b-P(MDO)<sub>71</sub> in CDCl<sub>3</sub>.

## Detailed MALDI-ToF MS analysis of mPEG<sub>48</sub> and mPEG<sub>48</sub>-b-P(MDO)<sub>15</sub>

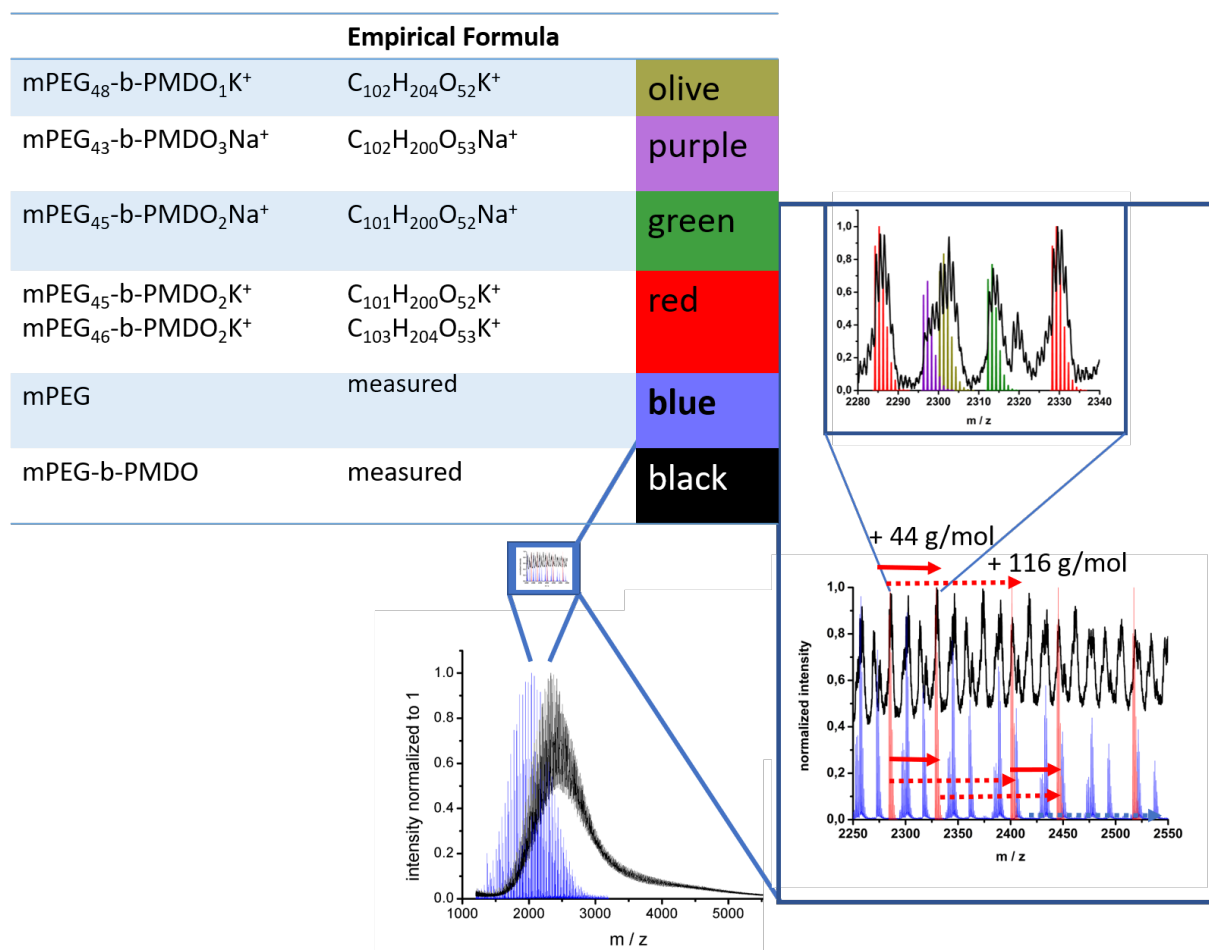


Figure S 30: Overlay of MALDI-ToF mass spectra of mPEG<sub>48</sub>-b-P(MDO)<sub>15</sub> and mPEG<sub>48</sub>. The magnified area shows peaks annotated in red that cannot be explained by homopolymer or free mPEG. All mass peaks follow single MDO units (116 g/mol) and single PEG units (44 g/mol) repetitively. By simulation, we did only observe few MDO units grafted onto mPEG. This may be explained by the sensitivity of P(MDO) to the measurement conditions of MALDI-ToF MS causing depolymerisation. Besides, polymers with higher molecular weights are often less efficiently ionized by MALDI-ToF MS and are, therefore, often underrepresented. This may also explain that for the MALDI-ToF MS of all mPEG<sub>48</sub>-b-P(MDO) block copolymers rather similar shifts in molecular weights could be observed, while SEC and NMR clearly proofed the formation of longer P(MDO) blocks.

## Block copolymer self-assembly:

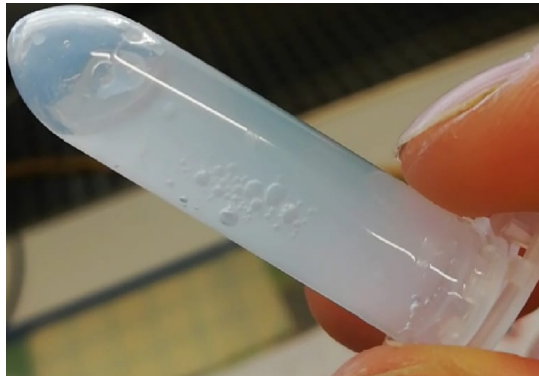
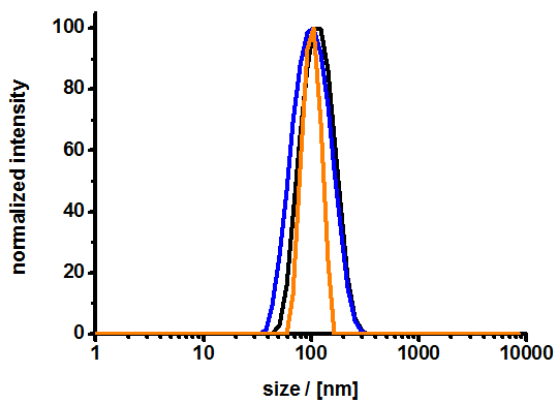


Figure S 31: Photograph of P(MDO) initiated by pyrene butanol in water. Homopolymer itself was even after vigorous mixing not soluble in water and still stuck to the wall of the Eppendorf tube or got slightly emulsified.

A:



B:

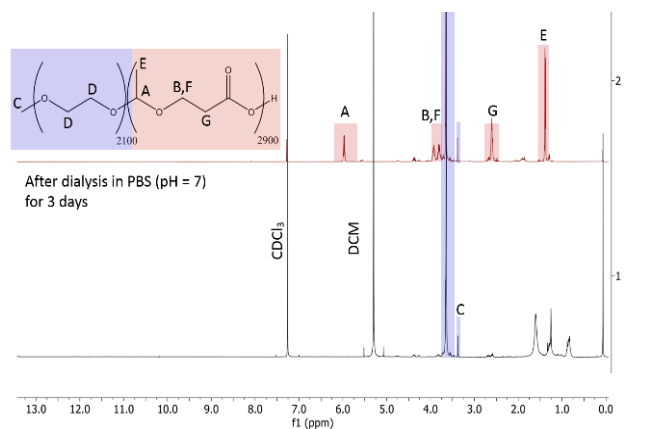


Figure S 32: A: Intensity size distribution of particles prepared from mPEG<sub>48</sub>-*b*-P(MDO) with different hydrophobic block lengths via solvent-switch method (dialysed for 8 h). B: <sup>1</sup>H-NMR of the extraction in CDCl<sub>3</sub> proves degradation into mPEG.

Table S1: Summarized data for preparation of micelles via solvent switch

	Diblock copolymer	Intensity mean	PDI
—	mPEG <sub>48</sub> - <i>b</i> -P(MDO) <sub>15</sub>	121 ± 2 nm	0,12
—	mPEG <sub>48</sub> - <i>b</i> -P(MDO) <sub>50</sub>	108 ± 5 nm	0,18
—	mPEG <sub>48</sub> - <i>b</i> -P(MDO) <sub>71</sub>	102 ± 5nm	0,4

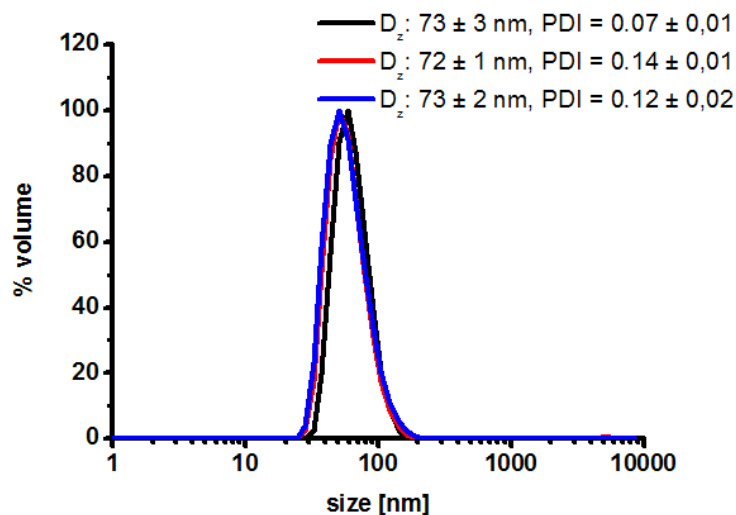


Figure S 33: DLS volume size distribution of micelles prepared from mPEG<sub>48</sub>-b-P(MDO)<sub>50</sub> via direct hydration technique. Micelles were independently prepared at different days. The Z-average diameter  $D_z$  was highly reproducible. DLS-measurements were conducted subsequently after preparation.

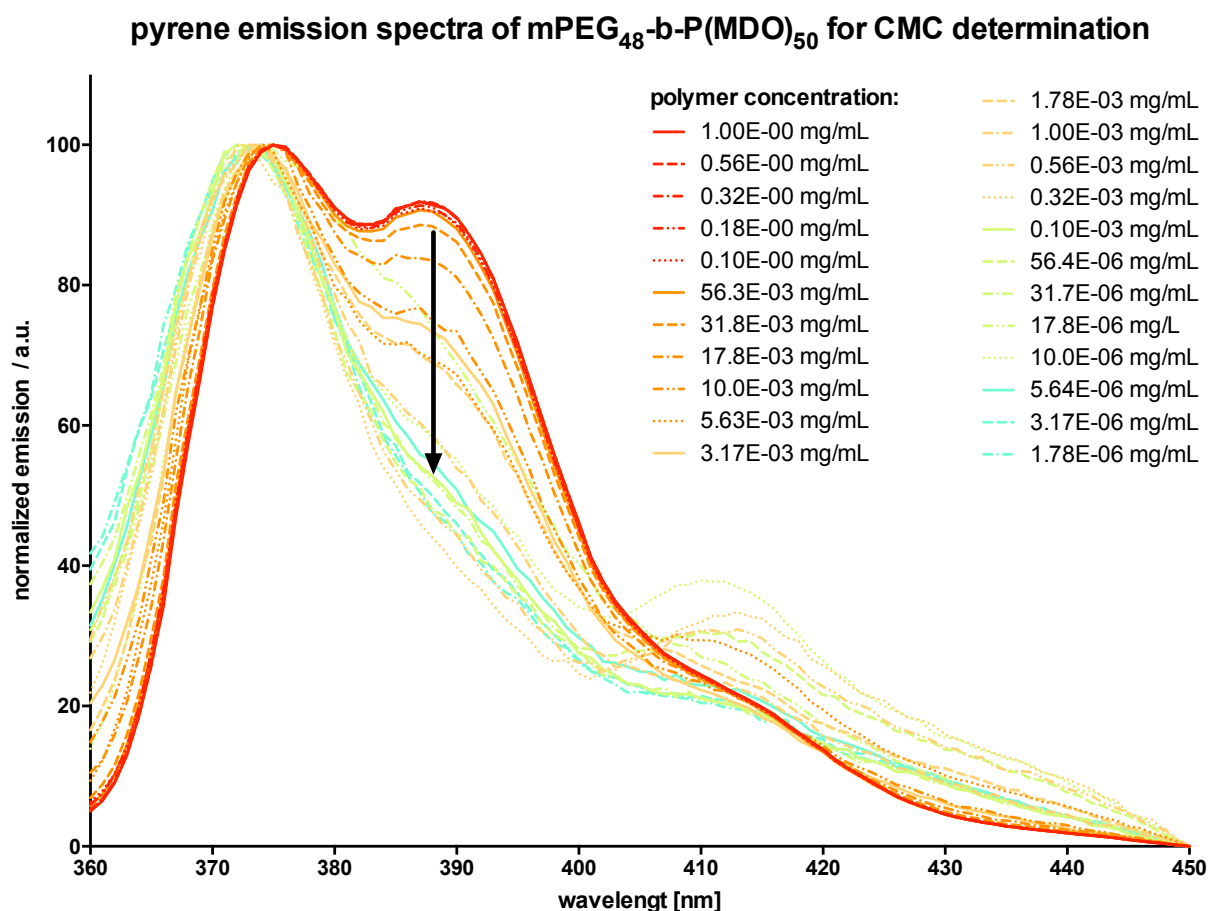


Figure S 34: Pyrene fluorescence emission spectra in presence of different concentrations of mPEG<sub>48</sub>-b-P(MDO)<sub>50</sub> in 10x PB buffer at pH 7. Not that the third vibronic band maximum  $I_3$  at 387 nm (in relation to its first vibronic band maximum  $I_1$  at 375 nm) is decreasing with decreasing concentrations of mPEG<sub>48</sub>-b-P(MDO)<sub>50</sub> and, thus, can be used to determine the polymers critical micelle concentration CMC (compare Figure S33).

results of the pyrene fluorescence ratio  $I_3/I_1$   
for various concentrations of  
 $mPEG_{48}\text{-}b\text{-}P(\text{MDO})_{50}$  and  $mPEG_{48}\text{-}b\text{-}P(\text{MDO})_{15}$

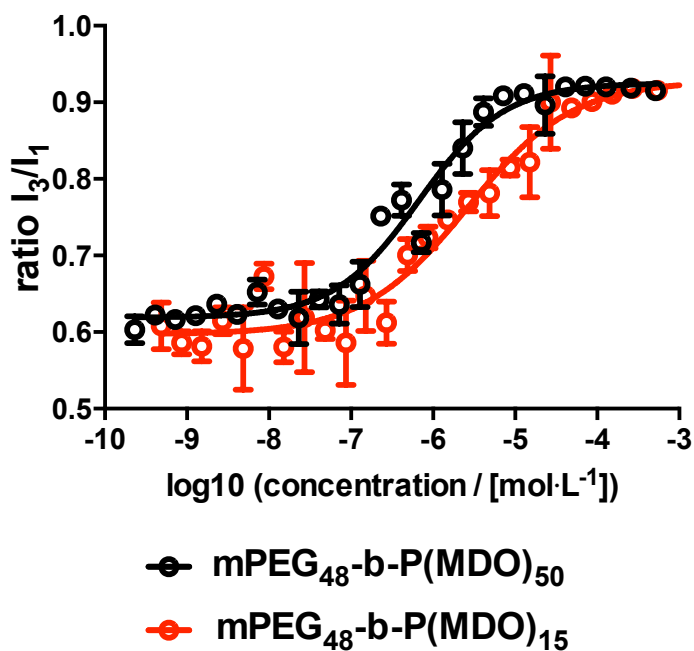
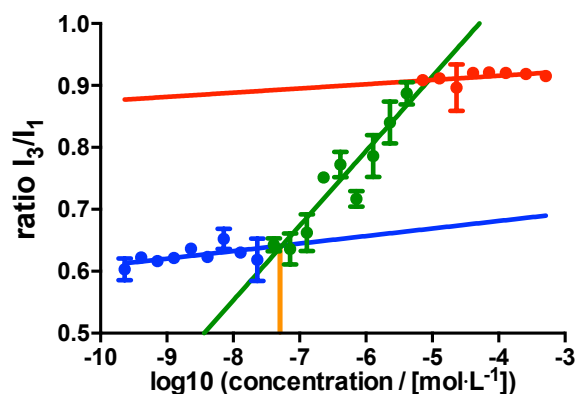


Figure S 35: Results of pyrene fluorescence emission ratio of third to first vibronic band maxima  $I_3/I_1$  for  $mPEG_{48}\text{-}b\text{-}P(\text{MDO})_{50}$  and  $mPEG_{48}\text{-}b\text{-}P(\text{MDO})_{15}$ , which can be used to determine the polymers' critical micelle concentration CMC (compare Figure S34 and S35). As all experiments were performed in aqueous media, hydrolytic polymer degradation cannot be avoided. Consequently, the derived CMC measurements (Figure S34 and S35) should be interpreted with caution, as during degradation all different lengths of block copolymers arise, which all vary in different CMC values individually. Moreover, due to the rapid sample preparation process, thermodynamic equilibria may probably not have been fully reached. Altogether, these results may only be used as orientation to compare the self-assembly properties of differently composed  $mPEG\text{-}b\text{-}P(\text{MDO})$  block copolymers.

**CMC determination of mPEG<sub>48</sub>-b-P(MDO)<sub>50</sub>  
by Pyrene fluorescence ratio I<sub>3</sub>/I<sub>1</sub>**

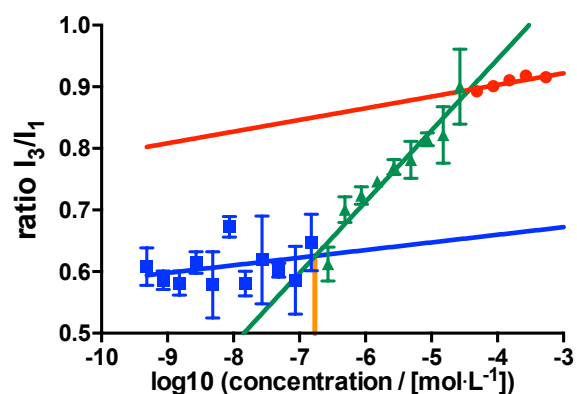


	1	2
m	0.1205 ± 0.01031	0.01216 ± 0.005172
b	1.517 ± 0.06612	0.7298 ± 0.04488

**log CMC = -7.27**  
**CMC = 54.2 nM**

Figure S 36: Results of CMC determination for mPEG<sub>48</sub>-b-P(MDO)<sub>50</sub>. Pyrene's I<sub>3</sub>/I<sub>1</sub> ratio was plotted versus logarithmic molar polymer concentration and linear extrapolations of steady ratio and increase ratio applied. Their intercepts we used to determine critical micelle concentration (CMC).

**CMC determination of mPEG<sub>48</sub>-b-P(MDO)<sub>15</sub>  
by Pyrene fluorescence ratio I<sub>3</sub>/I<sub>1</sub>**



	1	2
m	0.1157 ± 0.009993	0.01238 ± 0.009642
b	1.407 ± 0.05599	0.7093 ± 0.07898

**log CMC = -6.75**  
**CMC = 176.7 nM**

Figure S 37: Results of CMC determination for mPEG<sub>48</sub>-b-P(MDO)<sub>15</sub>. Pyrene's I<sub>3</sub>/I<sub>1</sub> ratio was plotted versus logarithmic molar polymer concentration and linear extrapolations of steady ratio and increase ratio applied. Their intercepts we used to determine critical micelle concentration (CMC).

## Dual pH-responsive degradation

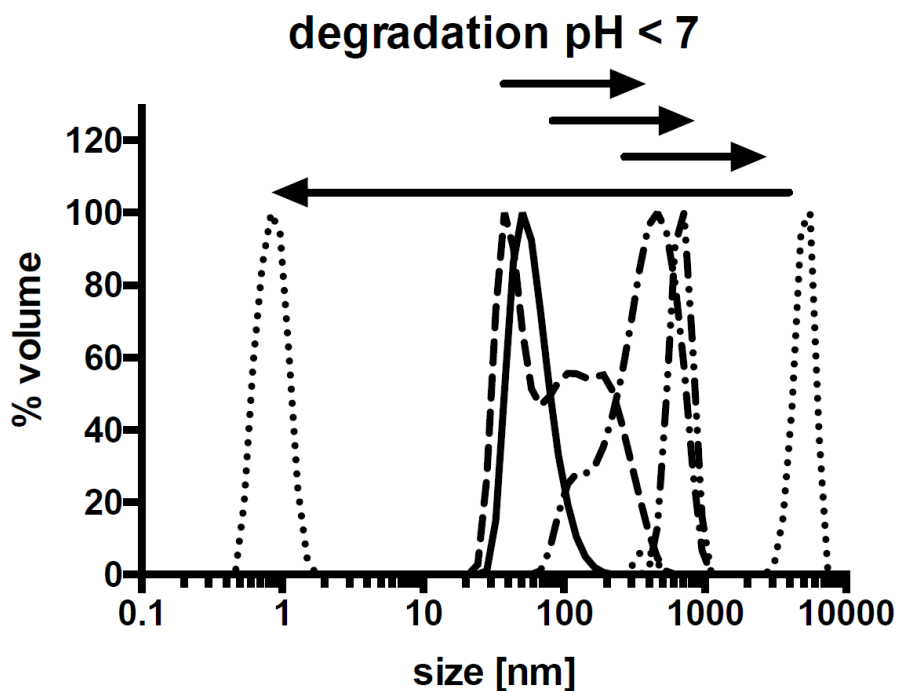


Figure S 38: Volume size distribution of micelles during degradation under acidic conditions. The size distribution at neutral pH is drawn as a solid line. Size distribution after addition of HCl are shown in dotted lines. Upon HCl addition (pH = 5.7), micelles first aggregate to micrometer-sized particles and then disassemble into small fragments.

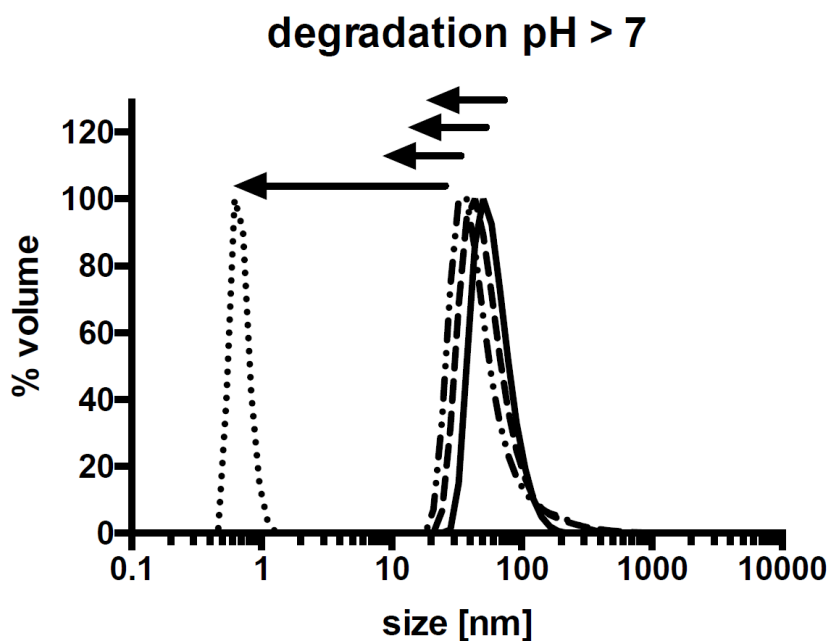


Figure S 39: Volume size distribution of micelles during degradation under basic conditions. The size distribution at neutral pH is drawn as a solid line. Size distribution after the addition of NaOH addition are shown in dotted lines (pH = 10.8). During degradation micelles slowly shrink into smaller aggregates until complete disassembly.

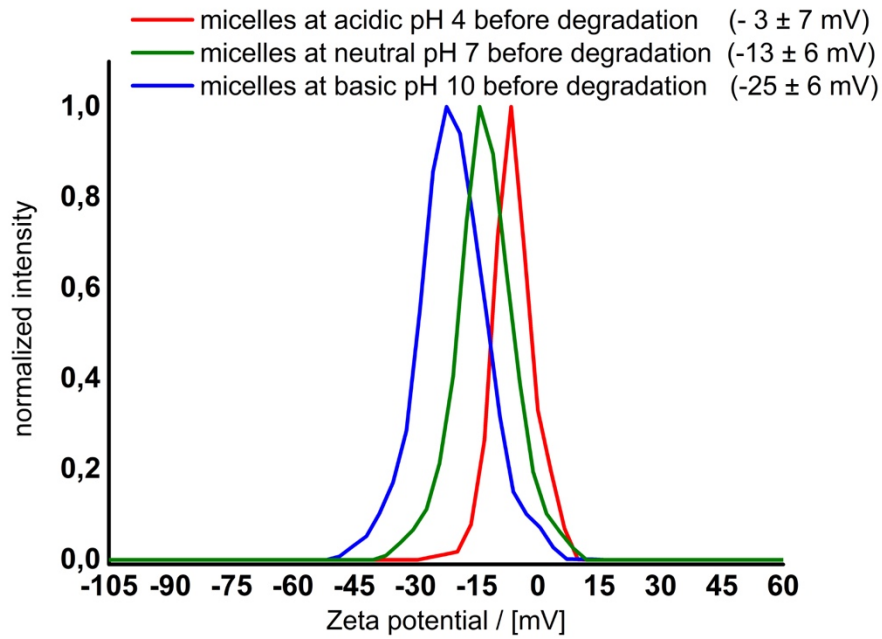


Figure S 40: Zeta Potential measurements of mPEG<sub>44</sub>-b-P(MDO)<sub>71</sub> micelles formulated in 5 mM HEPES buffer and adjusted to different pH levels.

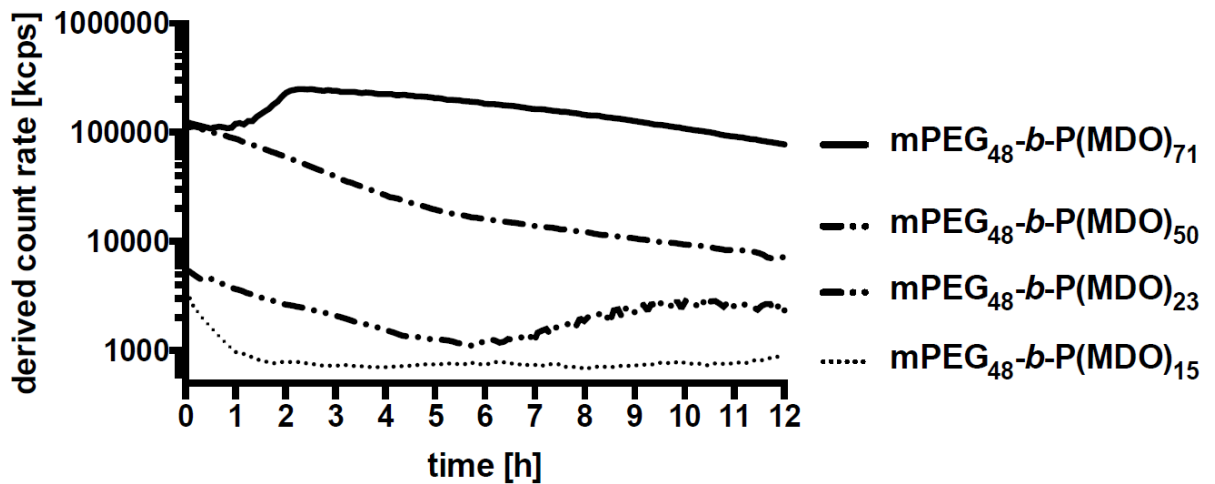


Figure S 41: Scattering intensity of particles over time for micelles prepared from mPEG<sub>44</sub>-b-P(MDO) with different hydrophobic block lengths by direct hydration technique. With increasing hydrophobic block lengths micelles exhibit increased stability, while the short blocks immediately disassembly already after 2 hours.

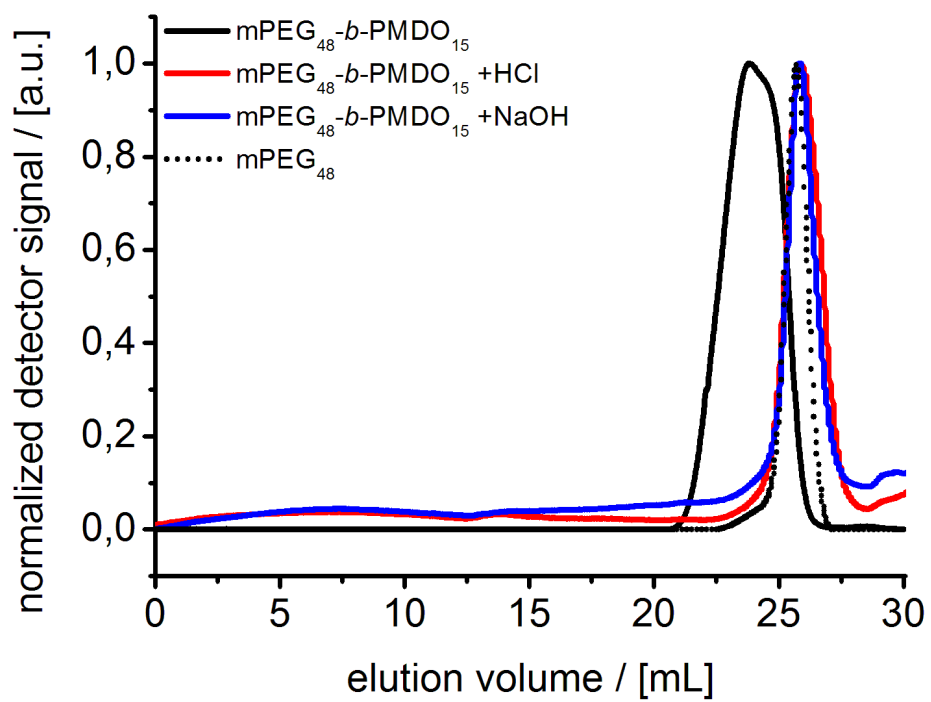


Figure S 42: THF SEC elugram of mPEG<sub>48</sub>-b-P(MDO)<sub>15</sub> after degradation under acidic and basic conditions. Experimental methods are explained in 2.7-c of the Materials and Methods section.

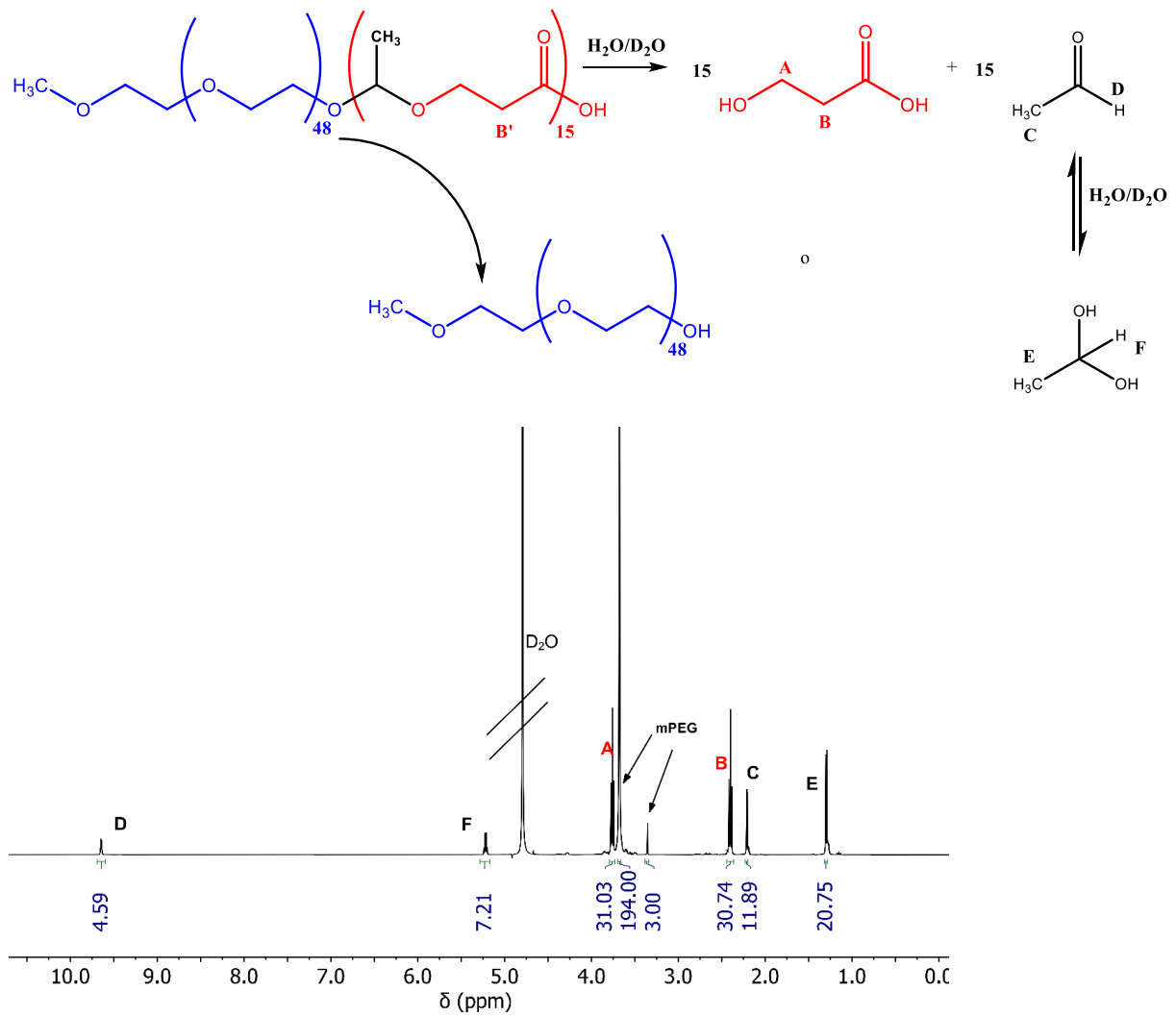


Figure S 43:  $^1\text{H}$  NMR (400 MHz) of degradation products of micelles prepared from  $m\text{PEG}_{48}\text{-}b\text{-P}(\text{MDO})_{15}$ .

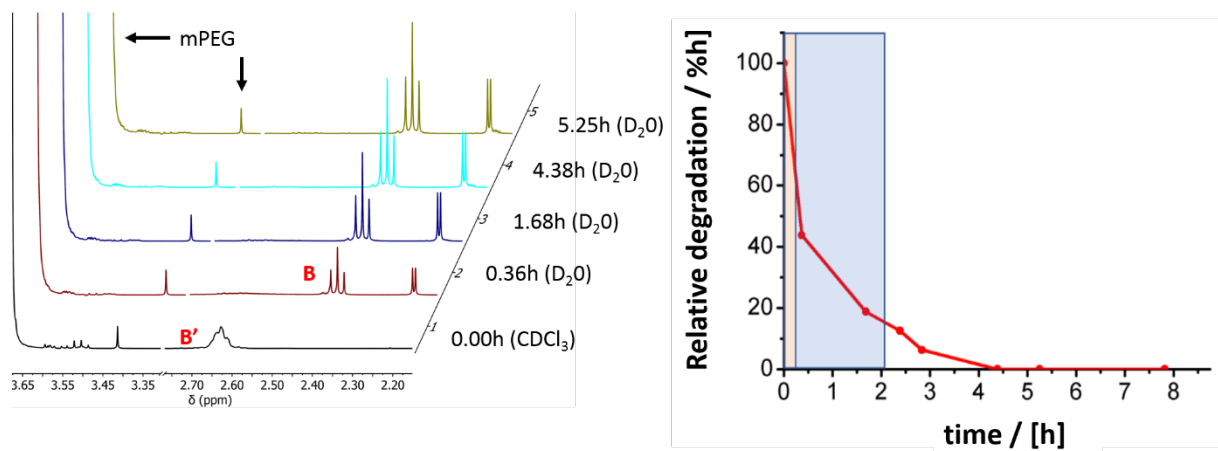


Figure S 44:  $^1\text{H}$ -NMR kinetic measurement of micelles prepared from  $m\text{PEG}_{48}\text{-}b\text{-P}(\text{MDO})_{15}$ . At sample preparation time was set to  $t = 0$  h. The red box marks the time frame interval of preparation. The blue box describes the time frame, in which disassembly of micelles was observed in DLS (compare Figure S41) confirming the dynamics of especially short P(MDO) blocks.

## Enzymatic degradation studies

- a) Enzymatic degradation of nonself-assembled block copolymers by solid-supported lipase in toluene

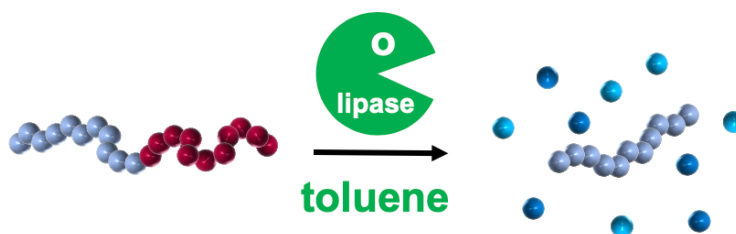


Figure S 45: Schematic representation of lipase mediated P(MDO) degradation of nonself-assembled of mPEG-*b*-P(MDO) copolymers in organic solvent (toluene).

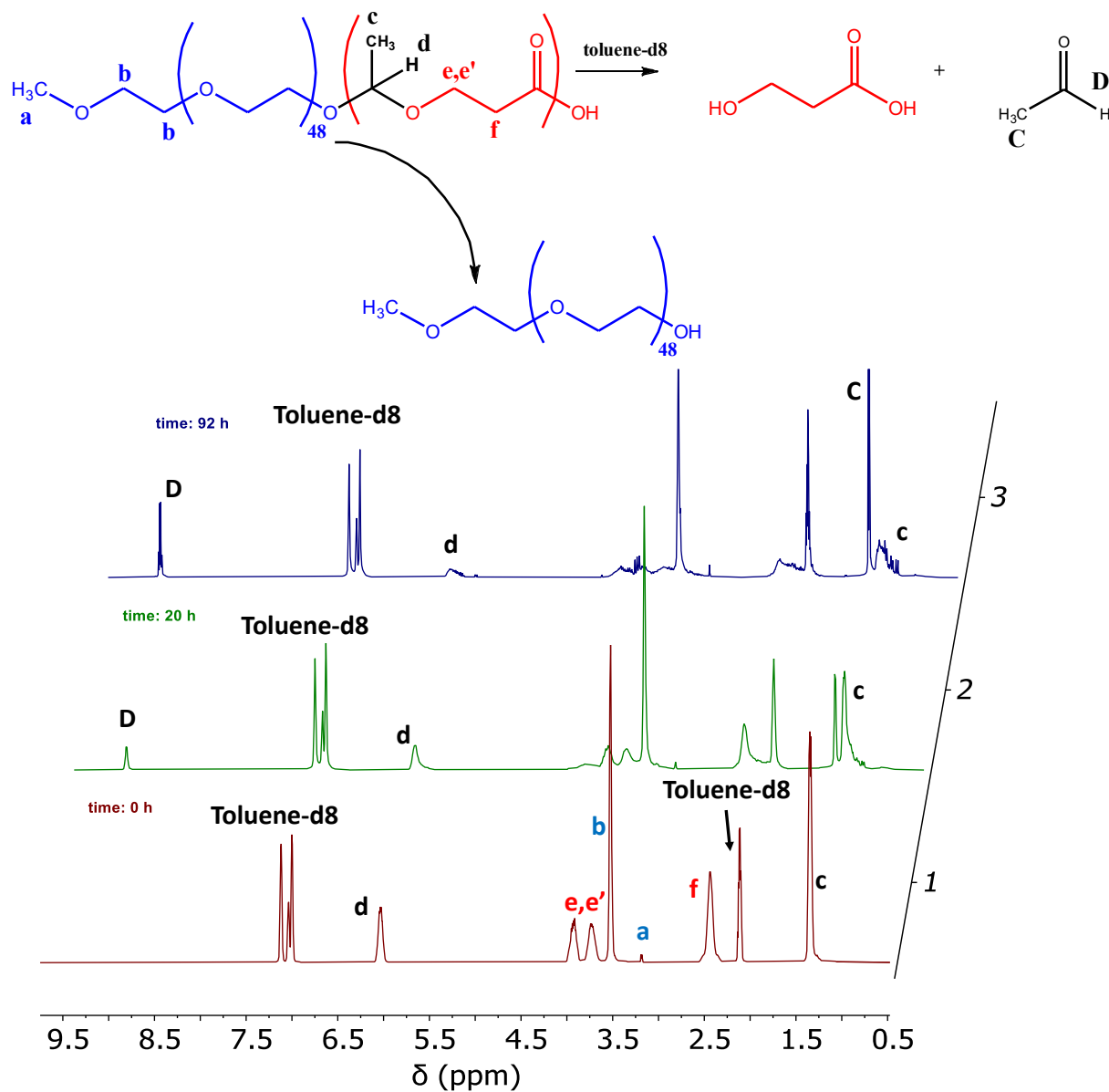


Figure S 46: <sup>1</sup>H-NMR kinetic measurement of mPEG<sub>48</sub>-*b*-P(MDO)<sub>71</sub> block copolymers in toluene-*d*<sub>8</sub>. At enzyme addition time was set to  $t = 0$  h. Signal D and d were used for calculating P(MDO) degradation (compare Figure S47).

## enzymatic degradation of mPEG<sub>48</sub>-*b*-PMDO<sub>71</sub> in toluene

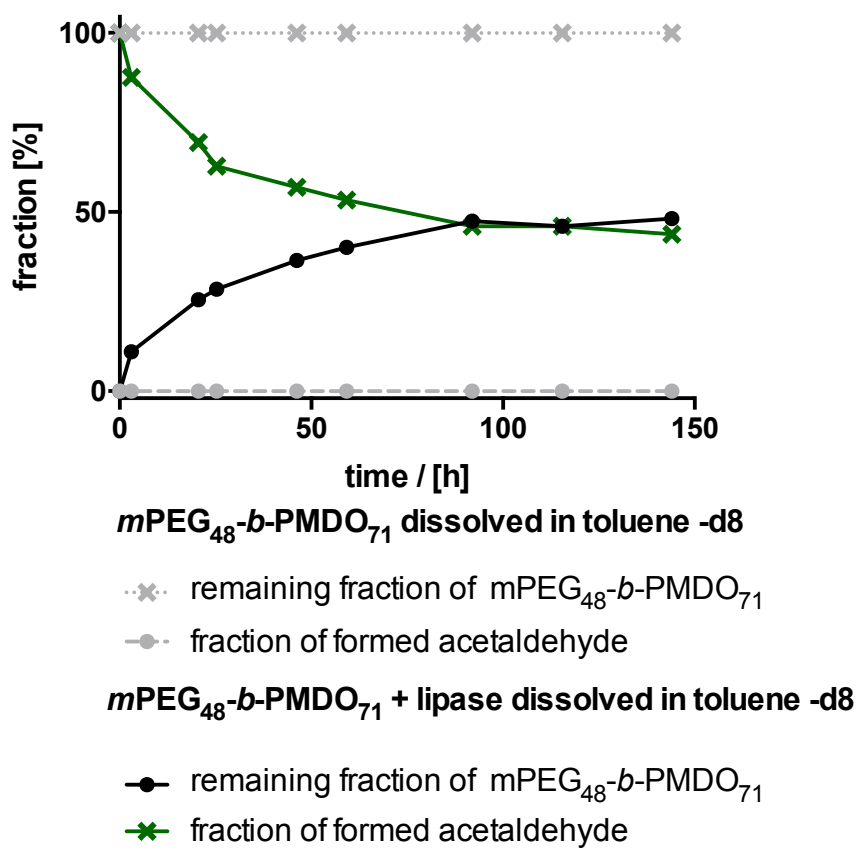


Figure S 47: Results of enzymatic P(MDO) degradation of mPEG<sub>48</sub>-*b*-P(MDO)<sub>71</sub> block copolymers in toluene-d8 determined by <sup>1</sup>H-NMR. Note that the P(MDO) block is fully stable in toluene over one week and is only degraded in presence of Novozyme 435 exclusively.

b) Enzymatic degradation of self-assembled micelles in pH7 buffered D<sub>2</sub>O monitored by solid-supported lipase B monitored via <sup>1</sup>H NMR and DLS

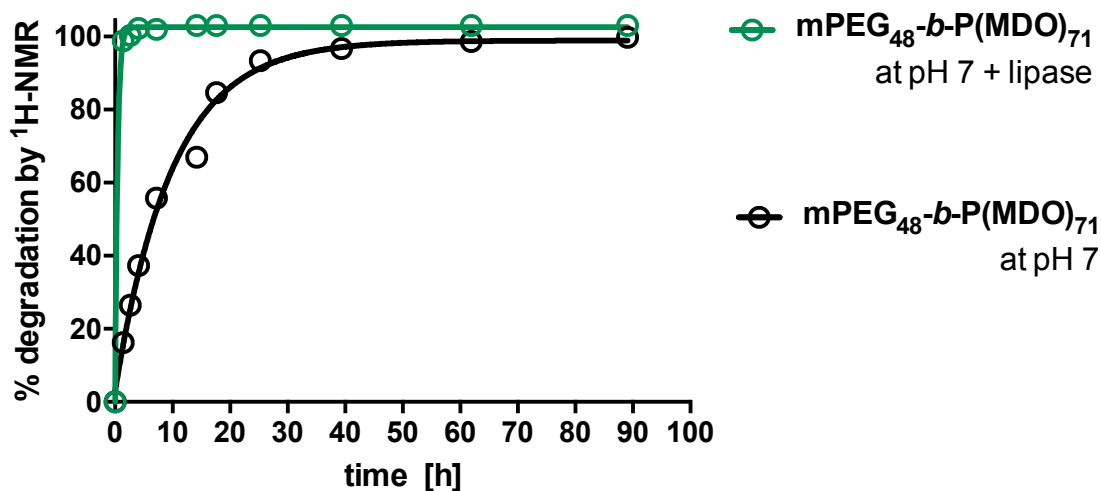


Figure S 48: Full view of the results from enzymatic P(MDO) degradation of mPEG<sub>48</sub>-b-P(MDO)<sub>71</sub> block copolymer micelles in D<sub>2</sub>O (120 mM phosphate) determined by <sup>1</sup>H-NMR (as shown in Figure 5). Note that compared to the rapid enzyme-mediated degradation a slow degradation in buffer without enzyme occurs over a longer time frame, too. In addition, although the proton resonance signals of the polymer backbone inside the micelle are suppressed, they still distort the proton signals of degradation products with similar chemical resonance shifts. Therefore, during the first 18 h the degradation was determined based on the arising aldehyde proton signals. They could be referenced to the singlet signal of dimethylsulfone (DMS) - both signals are shifted from any polymer signal and can be used for accurate peak integration/ calculation of P(MDO) degradation. After 26 h, the polymer was degraded more than 90% and no signal distortion was observed any longer. Degradation could then be derived from arising 3-hydroxypropionic acid, because at that time point minor evaporation of acetaldehyde cannot be excluded anymore. After complete degradation, we observed as many degradation products as expected based on the degree of polymerization. Moreover, we did not measure any further increase of degradation products over time. The signal proportion of mPEG to dimethylsulfone was confirmed after complete degradation.

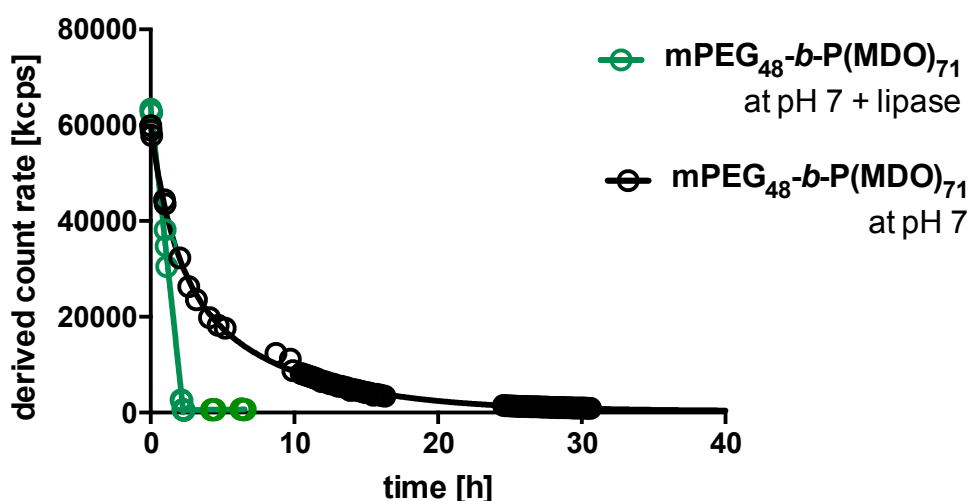


Figure S 49: Full view of the results from enzymatic P(MDO) degradation of mPEG<sub>48</sub>-b-P(MDO)<sub>71</sub> block copolymer micelles in 120 mM aqueous phosphate buffer determined by DLS (as shown in Figure 5). Note that compared to the rapid enzyme-mediated degradation a slow degradation in buffer without enzyme occurs over a longer time frame, too. The observed findings nicely correlate to the <sup>1</sup>H-NMR results shown in Figure S48.

## Loading and release studies

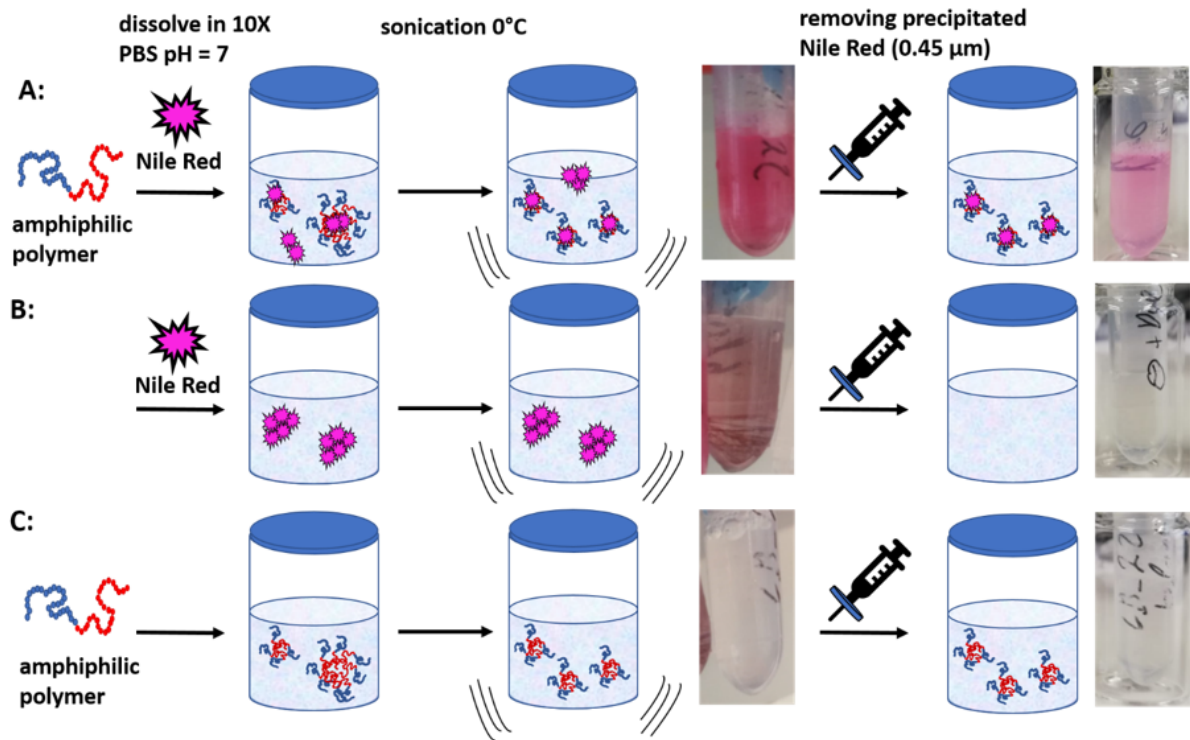


Figure S 50: Schematic overview of Nile Red encapsulation and corresponding negative controls without Nile Red and mPEG<sub>48</sub>-*b*-P(MDO)<sub>50</sub>. (A) To a defined amount of polymer the respective volume of Nile Red Stock solution was added and the solvent removed in vacuo. The residual material was dispersed in 120 mM phosphate buffer, assisted by 30 min sonication at 0°C. The resulting solution is displayed in A. Subsequently, the sample was filtered through a GHP-filter with a pore size of 450 μm in order to remove non-encapsulated, precipitated Nile Red dye. A clear pink solution with no visible aggregates was obtained. As controls, samples were prepared with Nile Red but no polymer (B) or polymer only but without Nile Red (C) and treated by ultrasound and filtration similarly.

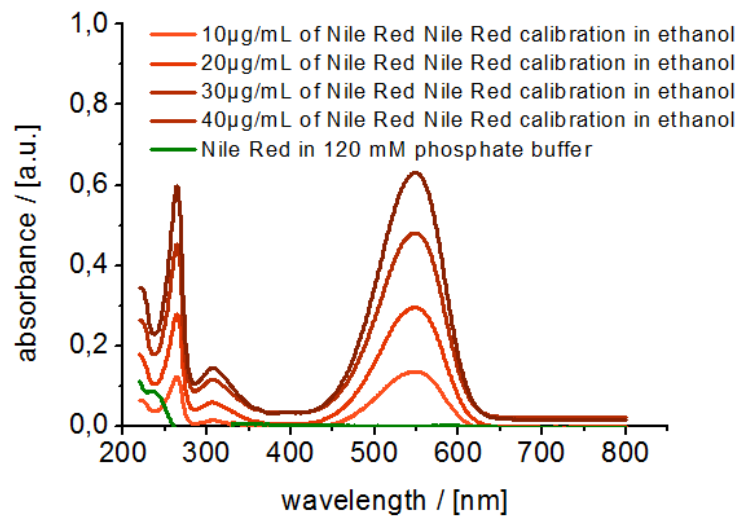


Figure S 51: UV/Vis spectra of Nile Red at different concentrations in ethanol and Nile Red in 120 mM phosphate buffer after filtration (where no dye is visible anymore).

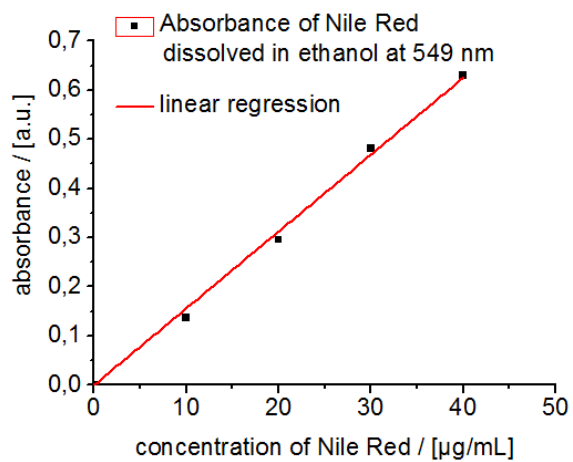
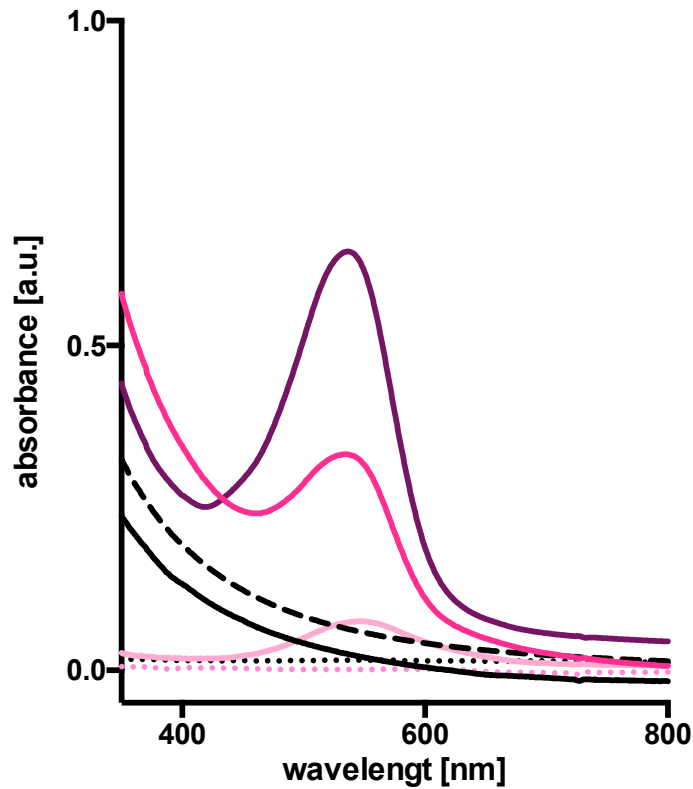


Figure S 52: External calibration curve for determining the Nile Red concentration.

$$A(549 \text{ nm}) = m \cdot c(\text{Nile Red})$$

$$m = \left( 15.64 \cdot 10^{-3} \frac{\text{mL}}{\mu\text{g}} \pm 0.27 \frac{\text{mL}}{\mu\text{g}} \right)$$



- .... empty mPEG<sub>48</sub>-b-P(MDO)<sub>15</sub> micelle
- Nile Red loaded mPEG-b-P(MDO)<sub>50</sub> micelle  
=> encapsulation efficiency 3.8%, dye loading 0.1 wt. %
- empty mPEG<sub>48</sub>-b-P(MDO)<sub>50</sub> micelle
- Nile Red loaded mPEG-b-P(MDO)<sub>50</sub> micelle  
=> encapsulation efficiency 19%, dye loading 0.5 wt. %
- empty mPEG<sub>48</sub>-b-P(MDO)<sub>71</sub> micelle
- Nile Red loaded mPEG<sub>48</sub>-b-P(MDO)<sub>71</sub> micelle  
=> encapsulation efficiency 36%, dye loading 0.9 wt. %
- .... Nile Red only and filtered

Figure S 53: UV/Vis absorbance spectra of different mPEG<sub>48</sub>-b-P(MDO) block copolymer micelles formulated with Nile Red and without. Note that with increasing P(MDO) block the amount of dye loading and encapsulation efficiency increases.

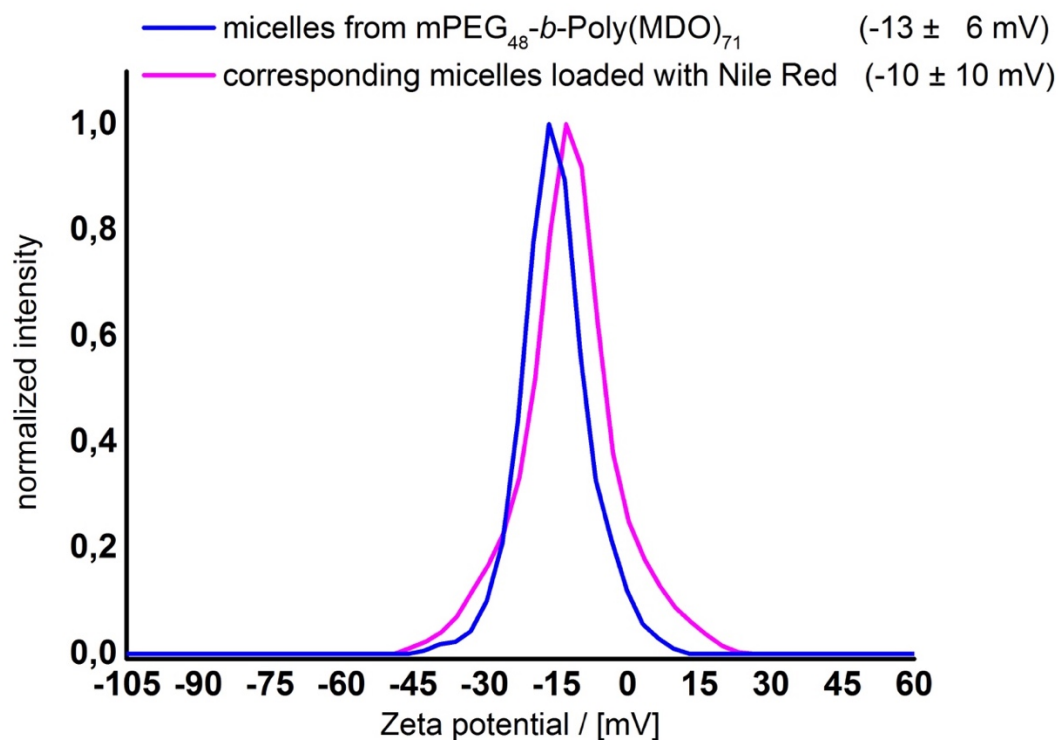


Figure S 54: Zeta Potential measurements of mPEG<sub>44</sub>-*b*-P(MDO)<sub>71</sub> micelles formulated with and without Nile Red loading in 5 mM HEPES buffer. Note that there is no significant difference between the dye loaded and empty micelles' zeta potential.

A: acidic

B: neutral

C: basic

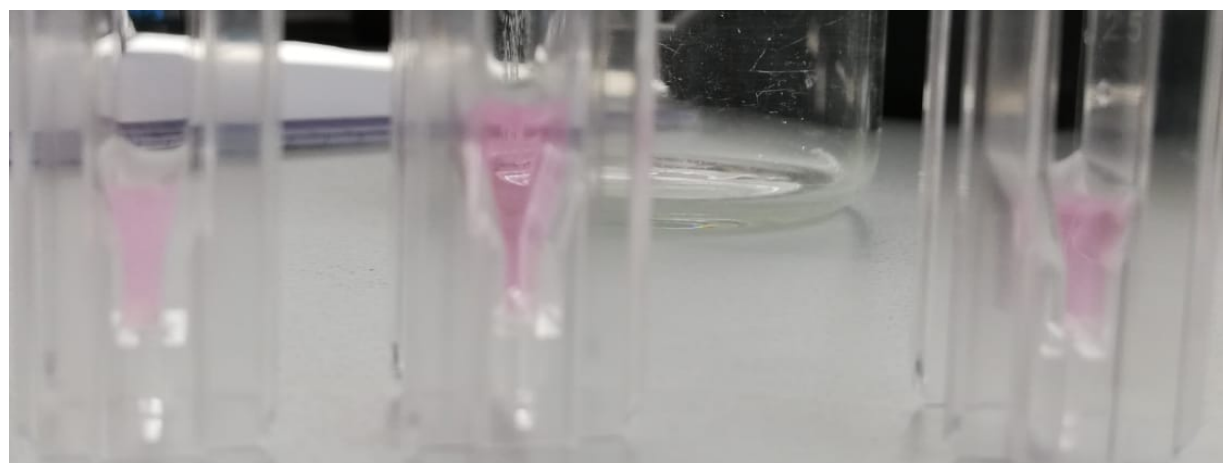
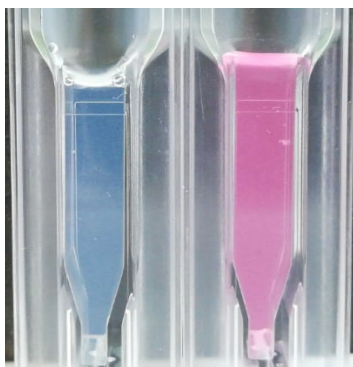


Figure S 55: pH-responsive behaviour of Nile Red loaded micelles. Again, micelles exposed to acidic conditions aggregate (left), which was not observed at neutral (center) and basic conditions (right). The observation was in agreement with non-loaded micelles shown in Figure 4.



Figure S 56: Acid-responsive behaviour of Nile Red loaded micelles. After exposure to acidic conditions (left) the P(MDO) degradation fragments heavily aggregate before they fully disassemble (as observed by DLS in Figure 4). During that process, Nile Red is somehow entrapped in the aggregates before it precipitates to the ground of the cuvette. Consequently, monitoring the absorbance of Nile Red cannot be performed accurately to correlate drug release from the degrading micelles. At pH 7 (right) the sample remains mostly transparent and released Nile Red slowly adsorbs to the ground of the cuvette.

before addition of lipase



after addition of lipase

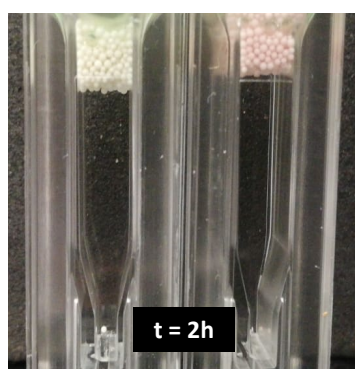
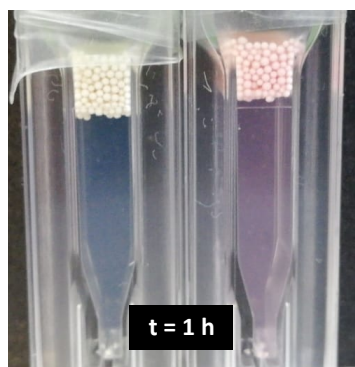
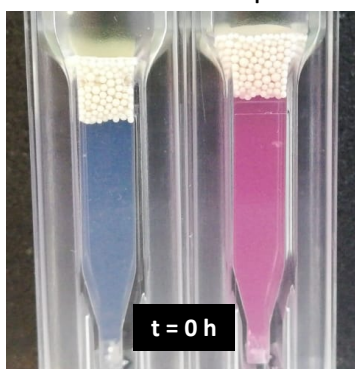


Figure S 57: Lipase-responsive behaviour of empty (left) and Nile Red loaded (right) micelles. After addition of resin-bound enzyme (floating on top of the aqueous media inside the cuvette) the P(MDO) degradation fragments do not aggregate but disassemble (as observed by DLS in Figure 4). During that process, released Nile Red is mostly adsorbing to the resin beads on top. Consequently, monitoring the absorbance of Nile Red as well as micelle scattering by DLS can be used to correlate drug release/ particle degradation easily.

## Application as immune drug delivery system

Table S 2: Dilution series of Adifectin formulated with polymer. The sample containing Adifectin without polymer were first treated in the same manner and expected to contain the same amount of amphiphilic drug as micellar formulation (its exact concentration of active TLR agonist was determined later on by Figure S61 and then fully corrected, as summarized by Table S 3 and shown in Figure S59 and S60).

sample c ( $\mu\text{M}$ )	stock	V ( $\mu\text{L}$ ) stock	PBS ( $\mu\text{L}$ )	dilution
40	40 $\mu\text{M}$	200	0	-
20	40 $\mu\text{M}$	100	100	1:1
10	20 $\mu\text{M}$	100	100	1 : 2
4	10 $\mu\text{M}$	80	120	1 : 2.5
2	4 $\mu\text{M}$	100	100	1 : 2
1	2 $\mu\text{M}$	100	100	1 : 2
0.4	1 $\mu\text{M}$	80	120	1 : 2.5
0.2	0.4 $\mu\text{M}$	100	100	1 : 2
0.1	0.2 $\mu\text{M}$	100	100	1 : 2
0.04	0.1 $\mu\text{M}$	80	120	1 : 2.5

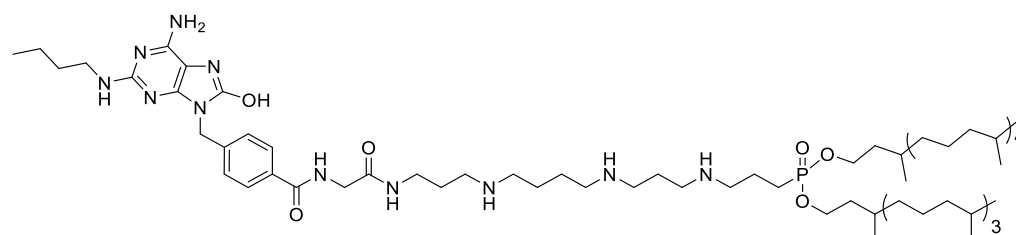


Figure S 58: Molecular structure of Adifectin with its TLR 7 interacting head group, a basic spermin linker, and two hydrophobic phytanyl groups.

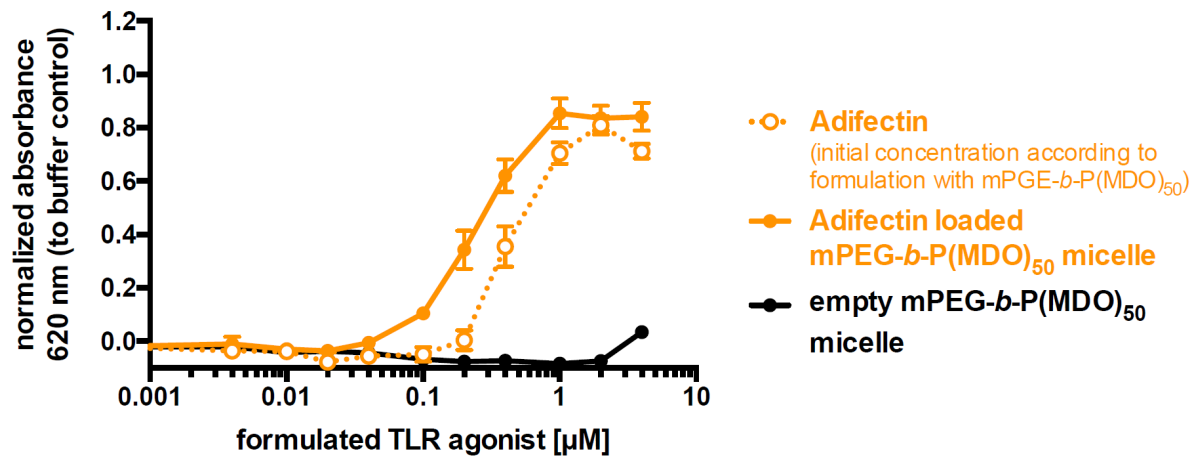


Figure S 59: TLR-stimulation on RAW Blue macrophages of Adifectin, which was formulated with or without mPEG<sub>48</sub>-*b*-P(MDO)<sub>50</sub>. Addition of empty mPEG<sub>48</sub>-*b*-P(MDO)<sub>50</sub> micelles served as controls.

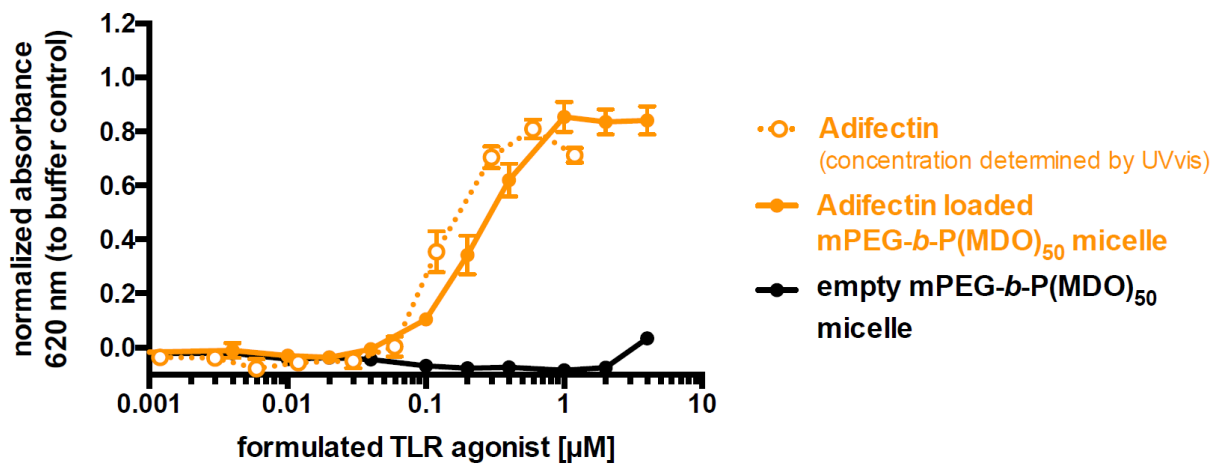
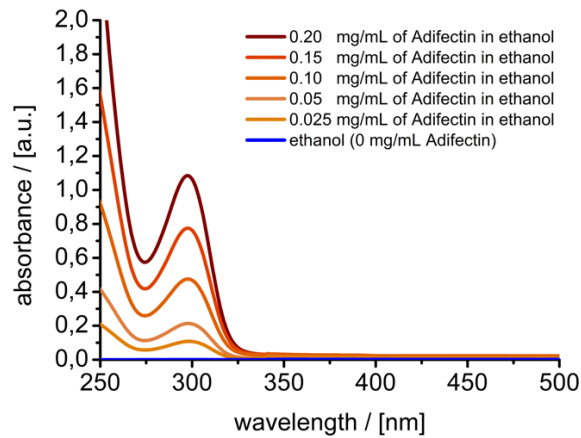
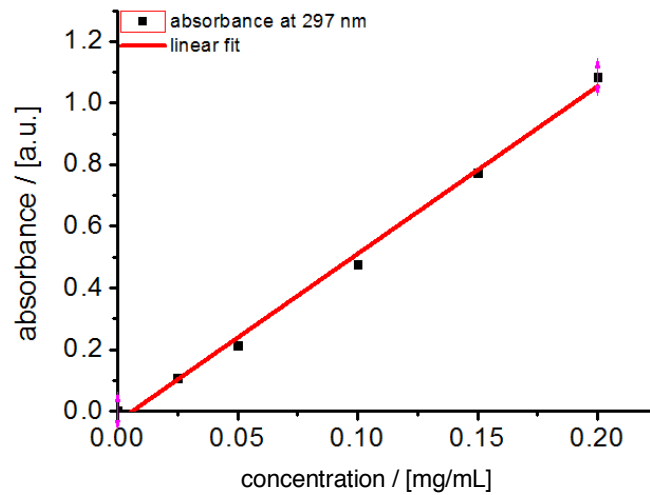


Figure S 60 TLR stimulation assay on RAW Blue macrophages evaluated by corrected TLR agonist concentration of the Adifectin sample without polymer determined by UV/Vis spectroscopy (compare Figure S61 and Table S3).

A:



B:



$$A(297\text{nm}) = m \cdot c(\text{Adifectin}) + b = 5.43955 \cdot c(\text{Adifectin}) \left[ \frac{\text{mg}}{\text{mL}} \right] - 0.03362$$

C:

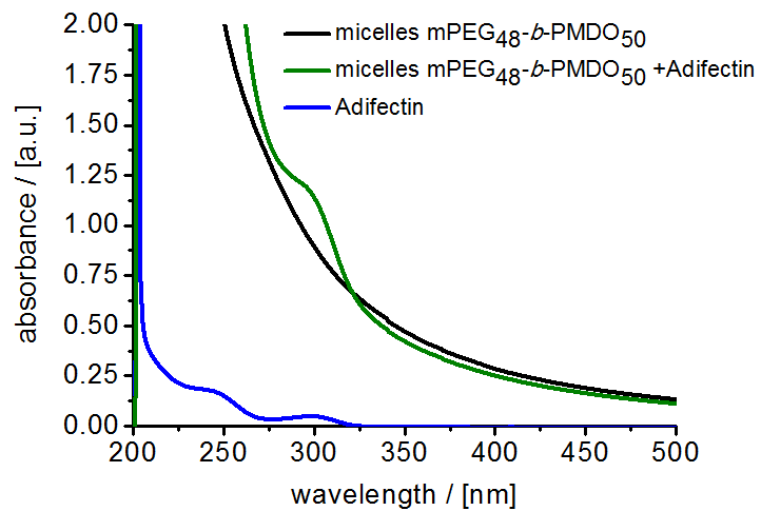


Figure S 61 A: UV/Vis spectra of Adifectin at different concentrations in ethanol. B: External calibration curve for determination of the Adifectin concentration. C: Absorbance spectra of Adifectin formulated with and without polymer, pure polymer micelles serve as reference for particle absorbance.  $\Delta A = 0.243 \Rightarrow c(\text{Adifectin}) = 50.9 \mu\text{g}/\text{mL}$  (for a 4 mg/mL polymer solution).

Table S 3: Corrected Adifectin concentration by UV/Vis quantification.

<b>Adifectin concentration determined in the polymer formulation sample c (<math>\mu\text{M}</math>)</b>	<b>Corrected concentration for the sample containing solely Adifectin sample c (<math>\mu\text{M}</math>)</b>
40	11.93
20	5.96
10	2.98
4	1.19
2	0.60
1	0.30
0.40	0.12
0.20	0.06
0.10	0.03
0.04	0.01